Petrological aspects of the Bayazeh Paleozoic ophiolite (Central Iran); implications for Paleo-Tethys subduction

Nargess Nosouhian [1], Ghodrat Torabi [1,*], Shoji Arai [2]

[1] Department of Geology, University of Isfahan, Isfahan, 81-7467-3441, Iran
[2] Institute of Liberal Arts and Science, Kanazawa University, 920-1192 Kanazawa, Japan

ABSTRACT

The Paleozoic Bayazeh ophiolite is situated in the western part of the Central-East Iranian Microcontinent (CEIM). This ophiolite consists of serpentinized peridotite, metagabbro, metapicrite, serpentinite and amphibole-bearing listwaenite, which are covered by schists and marbles. Serpentinites in the Bayazeh ophiolite are produced by serpentinization of a mantle protolith. The composition of primary chromian spinel cores (with average content of Cr~9.9, Mg~4.3, Ti< 0.01 and Fe^{3+}<0.5 apfu) in the Bayazeh serpentinites suggests an origin from high degrees of partial melting of a depleted harzburgite source in a supra-subduction zone setting. The texture and mineral assemblage of amphibole-bearing listwaenites and their association with serpentinites indicate that the studied listwaenites were generated by prograde metamorphism under upper greenschist to lower amphibolite facies conditions from a carbonated serpentinite. Geochemical characteristics of the Bayazeh metagabbros, indicate high value of large ion lithophile elements, high content of light rare earth elements, low HREE fractionations [e.g. $(Gd/Yb)_{CN}$=0.95-1.21], low contents of high-field strength elements and large variation of the LILE/HFSE ratios (e.g. Sr/Sm=47.83-564.67). These compositions are similar to cumulate gabbros and point to a possible role of melts from a lithospheric mantle and effect of fluids derived from the subducted slab in their formation. Mineralogical characteristics (e.g. presence of primary hydrous minerals such as phlogopite up to 10 vol%) and chemical composition of the Bayazeh metapicrites suggest derivation from a metasomatized asthenospheric mantle. Metasomatic enrichment of the mantle source probably occurred by fluids released during subduction of the Paleo-Tethys Ocean beneath the Central Iran. Subduction of the Paleo-Tethys from the Early to the Late Paleozoic is the cause of volatile enrichment and mantle metasomatism in the western part of the Central-East Iranian Microcontinent.

Keywords: Ophiolite; Supra-subduction zone; Paleo-Tethys; Paleozoic; Bayazeh; Central Iran.

INTRODUCTION

The lithological and chemical characteristics of ophiolitic complexes can provide useful information about the tectonic setting of their formation. Ophiolites can originate in mid-ocean ridge (MOR) and supra-subduction zone (SSZ) tectonic settings (e.g. Miyashiro, 1973; Pearce et al., 1984; Shervais, 2001; Van Hinsbergen

et al., 2015). The SSZ-type ophiolites are formed in back-arc basins and fore-arc extensional zones (Shervais, 2001; Wakabayashi et al., 2010; Van Hinsbergen et al., 2015). Depending on their structural characteristics the MOR-type ophiolites can be subdivided into slow-spreading and fast-spreading environments. It is generally assumed that the mantle peridotites of SSZ ophiolites mainly consist

PM

of harzburgite and the peridotites of MOR are essentially composed of lherzolite (e.g. Qiu et al., 2006).

The ophiolite complexes of Iran are a part of the Middle-East Tethyan ophiolite belt (Stocklin, 1968). These ophiolites link the Middle-Eastern and Mediterranean Hellenides-Dinarides ophiolites (e.g. Turkish, Troodos, Greek and Eastern European) to more easterly Asian ophiolites (Hassanipak and Ghazi, 2000). Iranian ophiolites are classified to the less abundance Paleozoic and the more abundance Mesozoic ophiolites (Arvin and Robinson, 1994). Remains of Paleo-Tethys Ocean crop out in the northern part of Iran and in the western part of the Central-East Iranian Microcontinent (CEIM), including the Anarak, Jandaq, Bayazeh and Posht-e-Badam ophiolites (Figure 1, Torabi et al., 2011). They are highly sheared, deformed and metamorphosed ophiolitic mélanges. The Bayazeh ophiolite is situated in the western part of the CEIM (Figure 1).

In this paper, the petrological and geochemical characteristics of the Bayazeh ophiolite are discussed.

Based on the results of field studies, petrography, mineral chemistry analyses and whole rock geochemistry about the Bayazeh ophiolitic sequence, we suggest petrogenesis and geotectonic setting of this important Paleozoic ophiolite in the CEIM. The sub-solidus evolutions in the lithological units of this ophiolite are also described.

GEOLOGICAL BACKGROUND

The main structural units of Iran and surrounding areas comprises separate continental blocks whose formation and evolution was controlled by the opening and closing of the Paleo-Tethys and Neo-Tethys oceans (Gansser et al., 1981; Bagheri, 2007). During the opening of the Neo-Tethys Ocean in the Late Paleozoic, several microplates were detached from northern Gondwana and attached to the southern Eurasia margin. Therefore, various branches of the Paleo-Tethys Ocean were closed along the northern margin and Central Iran (Bagheri, 2007; Bayat and Torabi, 2011).

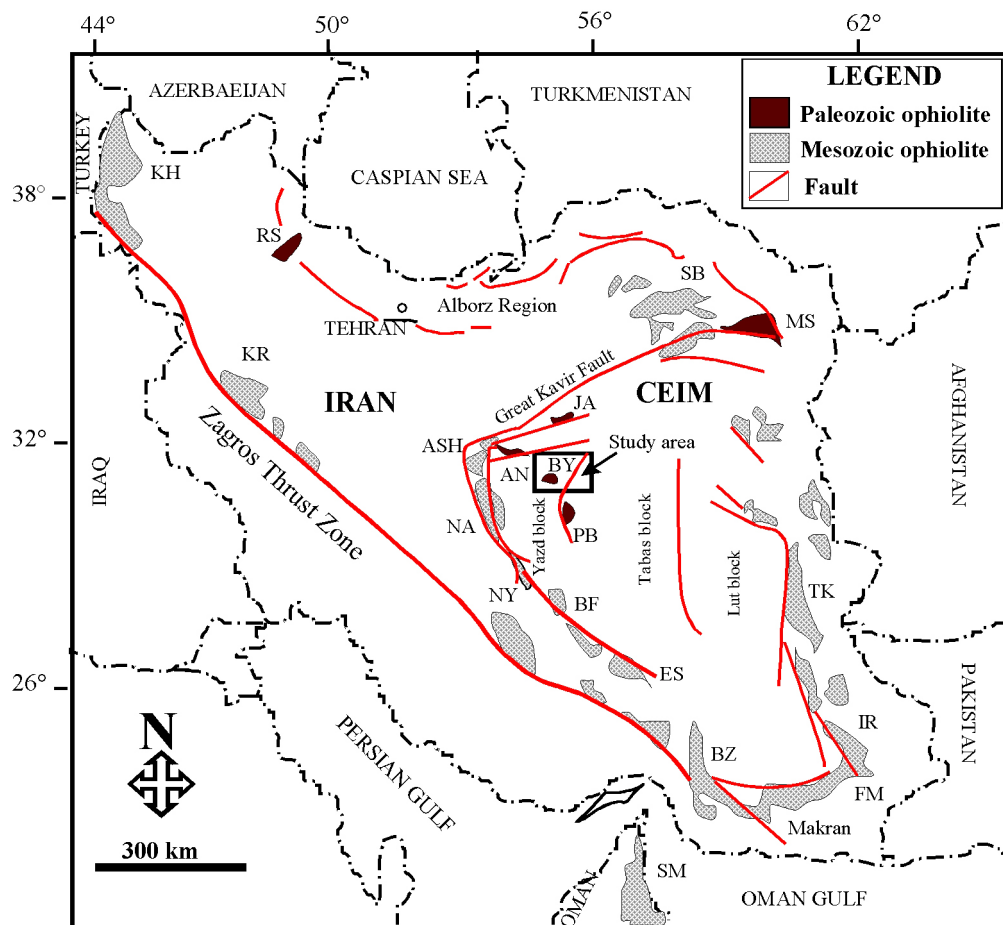The Iranian ophiolites can be divided into four groups

Figure 1. The main ophiolites of Iran (Torabi et al., 2011; slightly modified). KH= Khoy; KR= Kermanshah; NY= Neyriz; BZ= Band Ziarat; NA= Naein; BF= Baft; ES= Esphandagheh; FM= Fanuj-Maskutan; IR= Iranshahr; TK= TchehelKureh; MS= Mashhad; SB= Sabzevar; RS= Rasht; SM= Samail; ASH= Ashin; AN= Anarak; JA= Jandaq; BY= Bayazeh; PB= Posht-e-Badam.

(Torabi, 2013): 1. Mesozoic to Cenozoic ophiolites of the Zagros thrust zone, including the Neyriz and Kermanshah ophiolites; 2. Mesozoic to Cenozoic ophiolites and coloured mélanges along the CEIM border such as the Naein and Ashin ophiolites; 3. Paleozoic ophiolites of northern Iran along the Alborz mountain range, including the Rasht ophiolite, and 4. Paleozoic ophiolites within the Yazd and Posht-e-Badam blocks in the western part of the CEIM, including the Anarak, Jandaq, Bayazeh and Posht-e-Badam ophiolites (Figure 1). According to this, the first two categories are remnants of the Neo-Tethys Ocean, while the last two categories likely belong to the Paleo-Tethys (Torabi, 2012).

The CEIM is one of the major structural zones of Iran, which is located between the convergent Arabian and Eurasian plates. This microcontinent is bordered by major faults and Upper Cretaceous to Lower Eocene ophiolites that are remnants of the Neo-Tethys Ocean (Davoudzadeh, 1997). This microplate comprises four major tectonostratigraphic units, from east to the west (Figure 1), the Lut, Tabas (Kerman), Posht-e-Badam, and Yazd blocks (study area) (Stocklin, 1968). The CEIM structural units are characterized by distinct horst (e.g. Lut block) and graben (e.g. Kerman region) structures (Reichert, 2007).

The Yazd block is made up of highly sheared, deformed and metamorphosed ophiolitic mélanges of Paleozoic age (Nosouhian et al., 2016b). Several authors indicate that these ophiolites are remnants of the Paleo-Tethys Ocean with Paleozoic age (e.g. Davoudzadeh, 1997; Bagheri, 2007; Bagheri and Stampfli, 2008; Torabi, 2012; Nosouhian et al., 2014). ^{40}Ar-^{39}Ar muscovite dating show 320 to 333 Ma cooling ages for the metapelites covering the Central Iranian Paleozoic ophiolites (Bagheri and Stampfli, 2008). The U-Pb and ^{40}Ar-^{39}Ar analyses of the Pal-e-Havand area (SE of Anarak) metasediments yielded 262 and 255 Ma (Late Permian) ages, respectively (Bagheri and Stampfli, 2008). The Bayazeh ophiolite is situated in the eastern margin of the Yazd block (Figure 1). This ophiolite is located in the west of the Bayazeh village (south of Khur, Isfahan province) (Figure 2). The Turkmeni-Ordib, Bayazeh, Hajiabad and Chapedony faults are the main faults near the Bayazeh area and the studied ophiolite is exposed along the Bayazeh fault (Figures 2, 3). The Bayazeh ophiolite consists
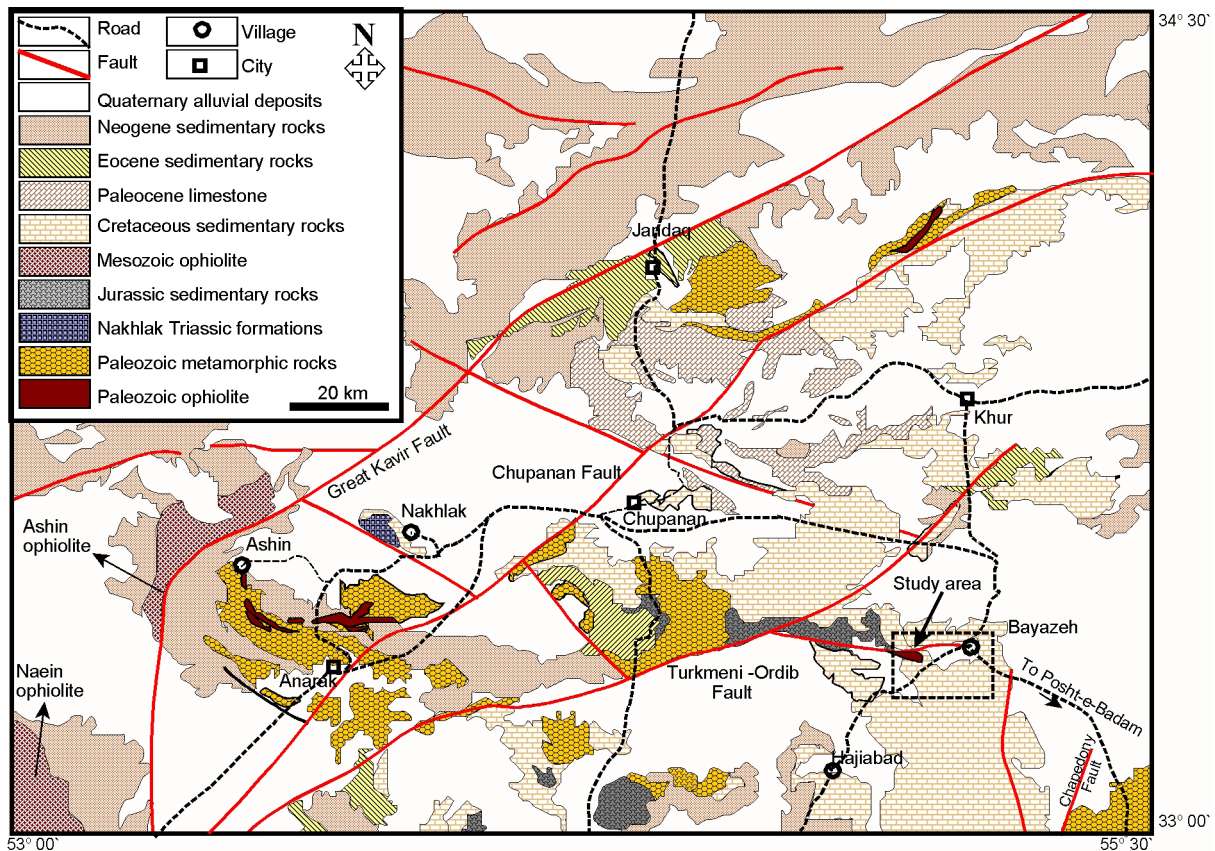

Figure 2. Simplified geological map of the Anarak- Khur- Jandaq- Bayazeh area, Isfahan province, Central Iran (Torabi and Arai, 2013; slightly modified). The studied ophiolite is situated in west of the Bayazeh village.

of serpentinized peridotites, metagabbro, metapicrite, serpentinite and amphibole-bearing listwaenite which are covered by Paleozoic schist and marble (Figure 4). The Bayazeh sequence and the covering metasediments are overlain by Cretaceous limestone, Neogene conglomerate and Quaternary alluvial deposits (Figures 3, 4). Alkali basalts with Late Paleozoic age are present in the southern part of the Bayazeh ophiolite, at the junction of the Bayazeh and Hajiabad faults (Figure 4A, G, Torabi and Hemmati, 2011). The presence of serpentinized peridotite and schist xenoliths with petrographic characteristics similar to the Bayazeh ophiolite units in the alkali basalts indicates that basalts cross cut the ophiolite (Torabi and Hemmati, 2011). Also, the Late Cretaceous dacitic dyke swarm cross cut the ophiolite and covering metamorphic rocks (Figure 4F, Nosouhian et al., 2016a).

Aistov et al. (1984) and Nosouhian et al. (2014, 2016b) suggested that the Bayazeh ophiolitic sequence and the metasediments underwent a progressive metamorphism under the upper greenschist to lower amphibolite facies P-T conditions, which was followed by a retrograde greenschist facies metamorphism.

ANALYTICAL METHODOLOGY

The rock-forming minerals of the Bayazeh ophiolitic rocks were analyzed with a JXA 8800, WDS (JEOL)

microprobe at the Kanazawa University, Japan. Analysis was performed under the following conditions: an accelerating voltage of 20 kV, a probe current of 20 nA, and a focused beam diameter of 3 μm. Composition of natural minerals and synthetic materials were used as standards. Each element was corrected by using the ZAF program. The Fe^{3+} and Fe^{2+} contents of minerals were calculated by assuming mineral stoichiometry (Droop, 1987). The $Cr\#=100\times Cr/(Cr+Al)$, $Mg\#=100\times Mg/(Mg+Fe^{2+})$, $Fe^{3+}\#=100\times Fe^{3+}/(Fe^{3+}+Cr+Al)$ and $Fe^{2+}\#=100\times Fe^{2+}/(Mg+Fe^{2+})$ were calculated for minerals. Representative chemical analyses of minerals and their calculated structural formula are listed in Tables 1 to 8.

The major and trace element compositions of Bayazeh metagabbro and metapicrite were obtained by a combination of Inductively Coupled Plasma Mass Spectrometry (ICP-MS) and Inductively Coupled Plasma Atomic Emission Spectroscopy (ICP-AES) methods at the Société Générale de Surveillance Company, Canada. The geochemical data of whole rock analyses are presented in Tables 9 and 10.

The trace element compositions of clinopyroxene from the metapicrite were determined by laser ablation system (193 nm ArF excimer: Geolas Q-Plus, MicroLas) coupled to an Agilent 7500s ICP-MS system at Kanazawa University, Japan. Analysis was performed based on the
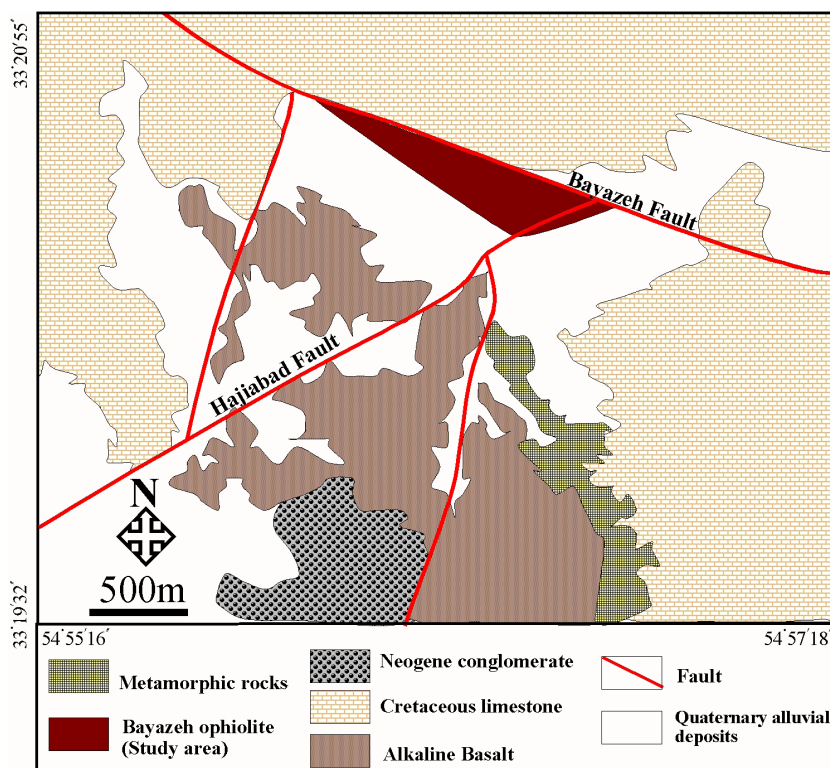
Figure 3. Simplified geological map of western part of the Bayazeh area, Central Iran.
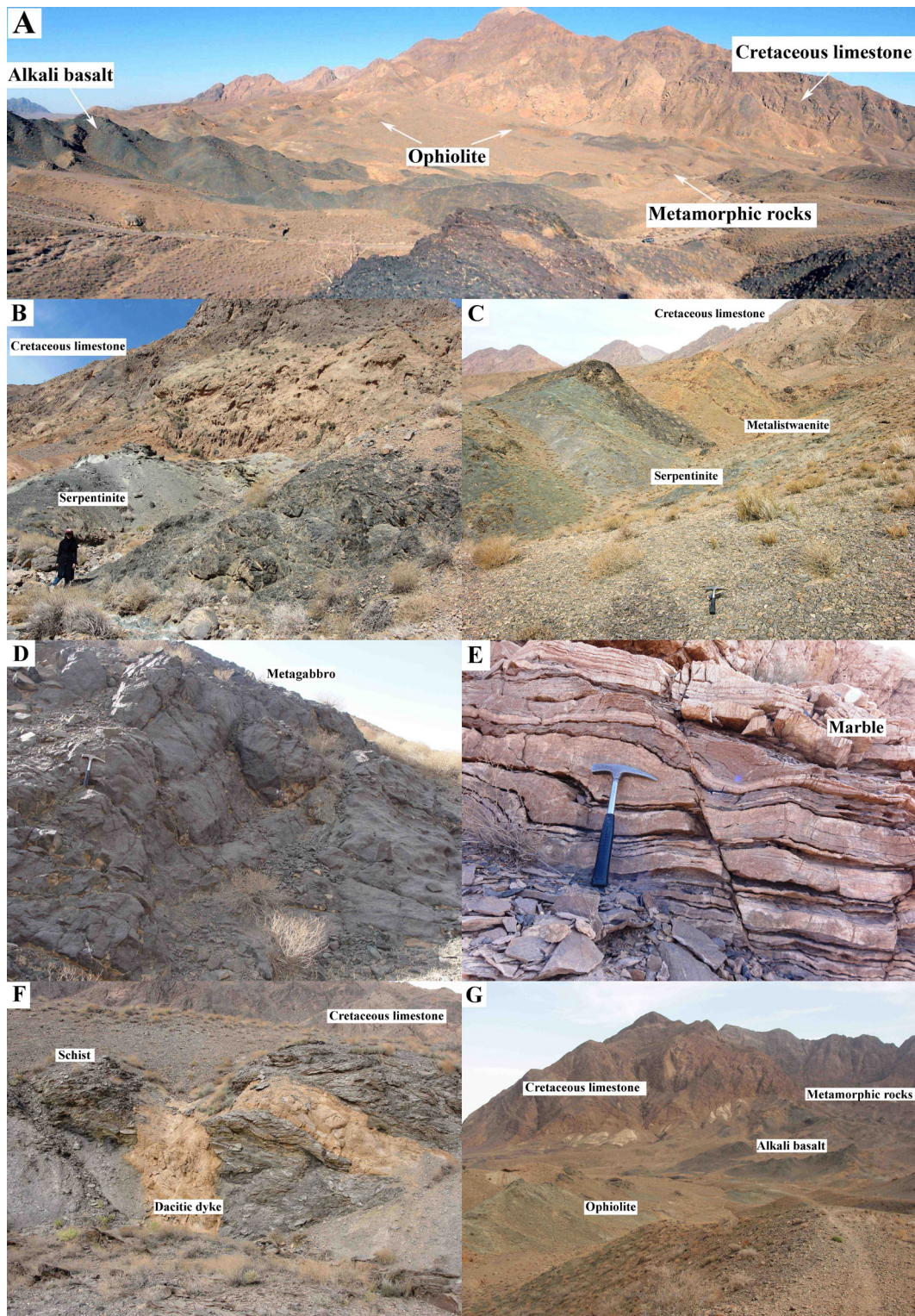
Figure 4. Field photos of the Bayazeh area. A) General view of the study area. B) Serpentinite is the most abundant rock unit of this ophiolite covered by metamorphic rocks and Cretaceous limestone. C) Exposure of the amphibole-bearing listwaenite vein associated with the serpentinite along the shear zones. Transitional change of serpentinite to the amphibole-bearing listwaenite is evident. D) Outcrop of the metagabbros in the Bayazeh ophiolite. E, F) The Bayazeh ophiolite is covered by metamorphic rocks such as schists and marbles. Dacitic dyke cross-cuts the schist. G) Alkali basalt in southern part of the study area cross cutting the Bayazeh ophiolite and metamorphic rocks.

method proposed by Morishita et al. (2005). According to this, the repetition rate and fluence of the laser ablation system were 6 Hz and 8 J/cm^2, respectively, and the laser-spot diameter was 60 μm for clinopyroxene. Table 10 shows the result of LA-ICP-MS analyses of minerals.

X-ray diffraction (XRD) analysis was achieved by XRD D8 advance, Bruker machine at the Central Laboratory of the University of Isfahan to typify the serpentine and carbonate minerals. Mineral abbreviations are those from Whitney and Evans (2010). Chromian spinel, labradorite, tremolitic-hornblende and pycnochlorite abbreviations are Cr-Spl, Lab, Tr-Hbl and Pyc, respectively.

PETROGRAPHY AND MINERAL CHEMISTRY
Serpentinized peridotite

Mantle peridotites in the Bayazeh ophiolite underwent high degrees of serpentinization (Figure 4 B,C). The serpentinization transformed the original mantle peridotites to serpentinized peridotite and serpentinite. Most of the original features of peridotites no longer exist, except for well-preserved chromian spinel cores. These minerals can be used to define the characteristics of the original mantle peridotite, as discussed in the 4.4 section.

Metagabbro

The Bayazeh metagabbros are compact, massive and medium- to coarse-grained (Figure 4D). Dioritic rocks are associated with gabbroic rocks. Unlike gabbro they are characterized by medium-grained, light color and increasing of quartz in the hand specimens. The Bayazeh gabbros have suffered sub-solidus evolutions consisting of sub-sea-floor metamorphism, hydrothermal alteration and regional metamorphism. According to this, most of the primary minerals of the gabbros are modified. The Bayazeh metagabbros present mainly granoblastic, nematoblastic and poikiloblastic textures (Figure 5 A,B). The rock-forming minerals are plagioclase, amphibole, epidote, chlorite, magnetite, calcite, quartz and titanite (Figure 5 A,B). The hydrothermal alterations in these rocks led to albitization and chloritization of the primary phases. Plagioclase is the main mineral in the Bayazeh metagabbros. Sub-sea floor metamorphism has changed the primary calcic plagioclase to secondary sodic ones (Figure 5B). Also, the effect of alteration process in the calcic plagioclase resulted in the formation of actinolite, albite, calcite and quartz, with minor epidote and chlorite (Figure 5A). The effect of progressive metamorphism under the upper greenschist to lower amphibolite facies product the metamorphic amphiboles with nematoblastic textures in these rocks. Most of the amphiboles are altered to chlorite, magnetite and titanite. Rock-forming minerals by stage of crystallization, texture, and hydrothermal

alteration in the Bayazeh ophiolite litological unites are listed in Table 11.

The electron microprobe analyses of minerals in the Bayazeh metagabbros show that plagioclases are labradorite (*An* 59 to 63) and albite (*An* 1 to 10) in composition (Table 1, Figure 6A). The primary calcic plagioclase is changed to secondary sodic ones and albites are restricted to products of alteration in the metagabbros. Amphiboles are actinolite (Figure 6B, Deer et al., 1992) with Mg# 59.48 to 69.87 (Table 2). They have low contents of TiO$_2$ (<0.07 wt%) and Al$_2$O$_3$ (1.10-4.05 wt%), supporting a metamorphic nature (Figure 6C, Veblen and Ribbe, 1982). Chlorite is pycnochlorite (Hey, 1954) with average Mg# of 75.86 (Table 2).

Metapicrite

Metapicrite is the most common rock-type in the Bayazeh ophiolite and the boundaries between the metapicrites and the other units in this complex are faulted. The Bayazeh metapicrites are extensively serpentinized and they are grayish-green to dark-green in outcrops. The main textures of these rocks are porphyroblastic and poikiloblastic (Nosouhian et al., 2014; Figure 5 C,D). The Bayazeh metapicrite consist of olivine (completely altered to serpentine), clinopyroxene, phlogopite, apatite, prehnite, amphibole, chlorite, ilmenite and magnetite (Figure 5 C,D). Olivine is the main phenocrystic phase in these rocks and completely altered to serpentine, minor amphibole, magnetite and chlorite (Figure 5 C,D). Clinopyroxene and phlogopite occur as relicts of the primary igneous minerals. They are nearly fresh phenocrysts and partly metamorphosed to chlorite, amphibole and opaque minerals (Figure 5 C,D). Plagioclase is completely altered to prehnite. Chromite is absent in these rocks. Matrix glass is significantly devitrified and chlorite is present throughout the matrix. Alteration processes in these rocks are serpentinization of olivine, chloritization of phlogopite, prehnitization of plagioclase and devitrification of glass (Table 11).

Microprobe analyses of minerals reveal that clinopyroxenes are diopside (Figure 6E, Morimoto, 1989); micas are phlogopite (Deer et al., 1992); amphiboles are tremolite, actinolite and tremolitic hornblende (Figure 6B, Deer et al., 1992); chlorites are clinochlore, penninite and diabantite (Hey, 1954), and opaque minerals are magnetite and ilmenite (Deer et al., 1992) in compositions (Nosouhian et al., 2014; Tables 3, 4, 5). Microprobe analyses reveal that primary igneous clinopyroxenes (Figure 6F, Berger et al., 2005) have Mg# of 86.60-92.52 and a wide range of TiO$_2$ (1.16-2.40 wt%) and Al$_2$O$_3$ (3.95-5.89 wt%) contents. The TiO$_2$ and Al$_2$O$_3$ contents of these minerals have positive correlation (Table 3). Phlogopites have FeO^{total}, TiO$_2$ and MgO contents of 8.54-10.07,
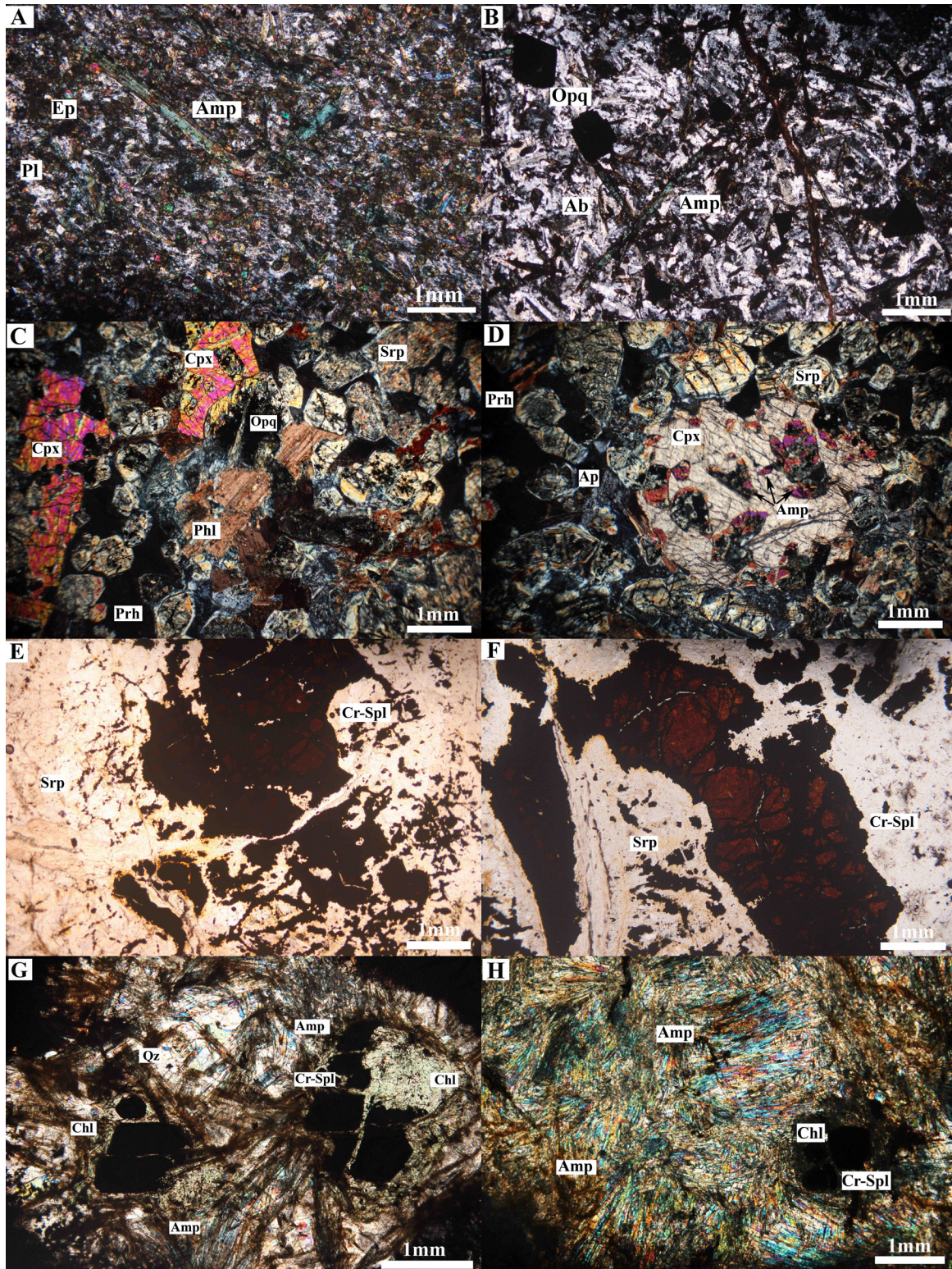
Figure 5. Photomicrographs of the Bayazeh rock units. A, B) Presence of sodic plagioclase and metamorphic amphiboles with minor epidote and magnetite in the metagabbros (XPL). C, D) Olivines completely altered to serpentine but clinopyroxene and phlogopite as primary and nearly fresh phenocrysts in the metapicrites (XPL). E, F) Subhedral chromian spinel with fresh cores and altered rim in the serpentinite (PPL). G, H) High amounts of metamorphic amphiboles with carbonate, quartz and relicts of chromian spinels altered to the ferritchromite and chlorite in the amphibole-bearing listwaenite (XPL).

Table 1. Representative chemical compositions of plagioclase (in wt%) in the Bayazeh metagabbros and their calculated structural formula.

Rock Type	Metagabbro								
Sample	N16-2	N16-4	N16-1	N23-1	N23-1	N23-2	N28-1	N28-2	N28-2
Point	9	11	6	13	16	18	22	24	25
Mineral	Lab	Lab	Ab	Ab	Ab	Ab	Ab	Ab	Ab
SiO_2	50.34	49.84	66.83	69.34	68.69	69.38	68.00	67.80	68.35
TiO_2	0.02	0.05	0.02	0.00	0.01	0.01	0.00	0.00	0.00
Al_2O_3	25.08	27.26	19.81	19.55	19.45	19.57	19.20	19.04	19.43
Cr_2O_3	0.00	0.00	0.00	0.00	0.00	0.00	0.02	0.00	0.00
FeO^{total}	3.26	3.47	0.55	0.06	0.08	0.06	0.12	0.09	0.13
MnO	0.06	0.03	0.01	0.00	0.02	0.00	0.00	0.00	0.01
MgO	0.14	0.93	0.01	0.00	0.01	0.00	0.00	0.00	0.00
CaO	15.23	13.40	1.46	0.10	0.12	0.05	0.05	0.02	0.12
Na_2O	5.57	3.19	10.79	11.65	11.72	12.12	11.68	11.56	11.58
K_2O	0.27	1.74	0.59	0.05	0.05	0.05	0.07	0.07	0.05
Total	99.97	99.92	100.06	100.75	100.16	101.25	99.11	98.58	99.67
Structural formula based on 8 equivalent Oxygens									
Si	2.369	2.333	2.944	3.003	2.996	2.996	2.998	3.003	2.995
Ti	0.001	0.002	0.001	0.000	0.000	0.000	0.000	0.000	0.000
$Al^{(IV)}$	1.290	1.403	1.028	0.997	0.999	0.995	0.997	0.993	1.003
$Al^{(VI)}$	0.000	0.000	0.000	0.000	0.000	0.000	0.000	0.000	0.000
Cr	0.000	0.000	0.000	0.000	0.000	0.000	0.000	0.000	0.000
Fe^{3+}	0.000	0.000	0.000	0.000	0.000	0.000	0.000	0.000	0.000
Fe^{2+}	0.129	0.136	0.020	0.002	0.003	0.002	0.004	0.003	0.005
Mn	0.002	0.001	0.000	0.000	0.001	0.000	0.000	0.000	0.000
Mg	0.010	0.065	0.001	0.000	0.000	0.000	0.000	0.000	0.000
Ca	0.768	0.675	0.069	0.005	0.006	0.002	0.002	0.001	0.006
Na	0.509	0.290	0.922	0.978	0.991	1.015	0.998	0.993	0.983
K	0.017	0.104	0.033	0.003	0.003	0.003	0.004	0.004	0.003
Sum	5.095	5.009	5.018	4.988	4.999	5.013	5.003	4.997	4.995
End Members:									
Albite	39.30	27.10	90.00	99.20	99.10	99.50	99.40	99.50	99.10
Anorthite	59.40	63.10	6.70	0.50	0.60	0.20	0.20	0.10	0.60
Orthoclase	1.30	9.80	3.30	0.30	0.30	0.30	0.40	0.40	0.30

7.21-8.13 and 16.97-18.23 (wt%), respectively (Table 3). Mineral chemistry of amphiboles indicates that all amphiboles compositions represent those of metamorphic amphiboles (Figure 6C, Veblen and Ribbe, 1982). They are tremolite, actinolite and tremolitic hornblende in composition with Mg# of 87.60-92.57, 78.49 and 92.25, respectively (Table 4). Serpentines have 1.47 to 4.56 wt% Al_2O_3 and Mg# in the range of 85.84-87.68 (Table 5). The XRD patterns of the analyzed metapicrites indicate that the serpentine minerals are antigorite (Nosouhian

et al., 2014). The antigorite is thought to have formed as a prograde product of lizardite and chrysotile during regional metamorphism (Moody, 1976).

The trace element compositions of clinopyroxenes in metapicrites were conducted by LA-ICP-MS analyses (Table 10). The chondrite-normalized REE patterns of clinopyroxenes show that all samples are enriched in LREEs (Figure 6G). The primitive mantle-normalized multi-element plots of clinopyroxenes indicate depletion in Ba, Th and U and negative anomalies of Pb, Sr, Ti and

Table 2. Representative chemical compositions of amphibole and chlorite (in wt%) in the Bayazeh metagabbros and their calculated structural formula.

Rock Type				Metagabbro							
Sample	N23-1	N23-1	N23-2	N23-2	N23-3	N28-1	N28-1	N28-2	Sample	N16-1	N16-1
Point	14	15	17	19	20	21	23	26	Point	5	7
Mineral	Act	Act	Act	Act	Act	Act	Act	Act	Mineral	Pyc	Pyc
SiO_2	52.56	52.58	51.54	51.53	49.61	54.91	53.36	54.70	SiO_2	29.94	28.52
TiO_2	0.07	0.03	0.05	0.04	0.05	0.03	0.03	0.00	TiO_2	0.01	0.01
Al_2O_3	3.68	3.25	3.77	4.05	2.50	1.77	2.72	1.10	Al_2O_3	19.06	20.21
Cr_2O_3	0.00	0.00	0.01	0.00	0.00	0.00	0.00	0.00	Cr_2O_3	0.03	0.00
FeO^{total}	19.59	19.04	17.55	18.23	18.56	16.38	18.03	14.09	FeO^{total}	13.44	13.88
MnO	0.32	0.30	0.25	0.28	0.29	0.31	0.26	0.21	MnO	0.23	0.29
MgO	10.49	10.95	11.52	11.61	11.45	13.16	11.95	14.99	MgO	24.34	23.83
CaO	6.72	6.75	9.28	8.22	7.83	9.13	8.25	11.36	CaO	0.22	0.04
Na_2O	3.76	3.67	2.49	3.00	3.34	2.01	2.51	0.87	Na_2O	0.03	0.01
K_2O	0.13	0.11	0.18	0.19	0.10	0.11	0.11	0.05	K_2O	0.00	0.00
Total	97.32	96.67	96.62	97.15	93.72	97.80	97.21	97.37	Total	87.30	86.78
Structural formula based on 23 equivalent Oxygens									Oxygens	28	28
Si	7.657	7.686	7.607	7.518	7.550	7.880	7.733	7.875	Si	5.920	5.696
Ti	0.007	0.003	0.005	0.004	0.006	0.003	0.003	0.000	Ti	0.001	0.001
$Al^{(IV)}$	0.343	0.314	0.393	0.482	0.448	0.120	0.267	0.125	$Al^{(IV)}$	2.080	2.304
$Al^{(VI)}$	0.288	0.246	0.262	0.213	0.000	0.179	0.197	0.061	$Al^{(VI)}$	2.358	2.448
Cr	0.000	0.000	0.001	0.000	0.000	0.000	0.000	0.000	Cr	0.004	0.000
Fe^{3+}	0.856	0.887	0.440	0.806	0.881	0.548	0.776	0.310	Fe^{3+}	0.000	0.000
Fe^{2+}	1.531	1.440	1.726	1.418	1.481	1.418	1.409	1.387	Fe^{2+}	2.223	2.317
Mn	0.040	0.037	0.031	0.035	0.037	0.038	0.031	0.025	Mn	0.039	0.049
Mg	2.278	2.387	2.534	2.524	2.597	2.814	2.583	3.217	Mg	7.175	7.094
Ca	1.049	1.057	1.468	1.285	1.276	1.404	1.281	1.752	Ca	0.047	0.008
Na	1.063	1.041	0.711	0.850	0.987	0.559	0.705	0.241	Na	0.010	0.005
K	0.024	0.020	0.033	0.035	0.020	0.020	0.021	0.010	K	0.001	0.000
Sum	15.136	15.118	15.212	15.170	15.283	14.983	15.006	15.003	Sum	19.858	19.922
Mg#	59.81	62.37	59.48	64.03	63.68	66.49	64.70	69.87	Mg#	76.35	75.38

Zr (Figure 6H). Negative Zr and Ti anomalies and low concentration of Rb, Ba, Th, U, Pb and Sr compared to primitive mantle indicate that the melt crystallizing the clinopyroxene have the mantle origin (e.g. Wang and Gasparik, 2001).

Serpentinite

Serpentinite is the most abundant litological unit of the Bayazeh ophiolite and present in all parts of this complex. The Bayazeh serpentinites are characterized by sheared massive appearance, grayish-green to dark-green in colour and wax-like luster (Figure 4 B,C). The transitional change of serpentinite to amphibole-bearing listwaenite is evident in the field observations. Petrographical studies of the serpentinites indicate that the main texture is mesh texture (Table 11). Mineral association of the serpentinite in the Bayazeh ophiolite is serpentine, chromian spinel, magnetite, chlorite, tremolite and actinolite (Figure 5 E,F). The serpentine with a fibrous flake morphology is the main mineral of these rocks, formed after olivine and pyroxene (Nosouhian et al., 2016b). Pseudomorphic bastite after orthopyroxene suggests a harzburgite protolith. XRD patterns of these rocks suggest that the serpentine polytype is antigorite.

Microprobe analyses of serpentine indicate low contents of Al_2O_3 (0.21-0.48 wt%) and high values of Mg# (98.30-

Table 3. Representative chemical compositions of clinopyroxene and phlogopite (in wt%) in the Bayazeh metapicrites and their calculated structural formula (Nosouhian et al., 2014).

Rock Type								Metapicrite						
Sample	B460-2	N11	N11	N11	N11	N11	N11-1	B460-2	B460-2	N11	N11-1	N11-1	N11-3	N11-6
Point	191	200	201	202	203	204	34	179	184	198	32	33	40	50
Mineral	Di	Di	Di	Di	Di	Di	Di	Phl	Phl	Phl	Phl	Phl	Phl	Phl
SiO_2	50.84	48.97	49.76	50.06	50.35	49.49	49.56	37.35	37.70	37.36	36.66	36.08	36.78	37.56
TiO_2	1.16	1.41	1.39	1.22	1.98	2.40	1.54	7.96	7.70	7.63	7.91	8.13	7.67	7.21
Al_2O_3	3.95	5.89	5.81	5.31	4.03	4.86	4.13	14.67	14.31	14.80	14.53	14.82	14.87	13.50
Cr_2O_3	0.54	0.76	0.73	0.68	0.15	0.11	0.39	0.02	0.09	0.00	0.01	0.02	0.03	0.00
FeO^{total}	4.98	5.16	5.06	5.24	5.14	5.30	5.00	8.61	8.67	8.87	8.54	8.86	8.58	10.07
MnO	0.09	0.08	0.13	0.08	0.09	0.09	0.09	0.06	0.05	0.05	0.03	0.07	0.05	0.17
MgO	15.24	14.38	14.57	14.53	14.75	14.67	15.24	17.35	17.80	17.27	17.96	16.97	17.11	18.23
CaO	23.50	22.76	22.75	22.95	22.75	22.58	22.84	0.01	0.00	0.03	0.01	0.01	0.04	0.05
Na_2O	0.36	0.30	0.32	0.36	0.62	0.55	0.42	1.07	1.09	1.08	1.01	1.08	1.04	0.74
K_2O	0.00	0.00	0.01	0.01	0.00	0.00	0.00	8.19	8.45	8.00	7.66	8.08	8.25	8.31
Total	100.65	99.73	100.53	100.47	99.89	100.07	99.20	95.28	95.85	95.07	94.31	94.11	94.42	95.83
	Structural formula based on 6 equivalent Oxygens							Structural formula based on the 22 equivalent Oxygens						
Si	1.855	1.807	1.821	1.834	1.853	1.820	1.833	5.405	5.433	5.416	5.351	5.306	5.378	5.450
Ti	0.032	0.039	0.038	0.034	0.055	0.066	0.043	0.866	0.834	0.832	0.868	0.899	0.843	0.787
$Al^{(IV)}$	0.145	0.193	0.179	0.166	0.147	0.180	0.167	2.500	2.429	2.526	2.498	2.566	2.560	2.306
$Al^{(VI)}$	0.025	0.063	0.072	0.063	0.028	0.031	0.013	0.000	0.000	0.000	0.000	0.000	0.000	0.000
Cr	0.015	0.022	0.021	0.020	0.004	0.003	0.011	0.003	0.010	0.000	0.001	0.003	0.003	0.000
Fe^{2+}	0.086	0.110	0.123	0.119	0.110	0.111	0.068	1.042	1.045	1.076	1.042	1.089	1.049	1.221
Fe^{3+}	0.066	0.049	0.032	0.042	0.048	0.052	0.087	0.000	0.000	0.000	0.000	0.000	0.000	0.000
Mn	0.003	0.003	0.004	0.002	0.003	0.003	0.003	0.007	0.005	0.006	0.004	0.009	0.006	0.020
Mg	0.829	0.791	0.795	0.793	0.809	0.805	0.841	3.744	3.824	3.732	3.908	3.721	3.730	3.942
Ca	0.919	0.900	0.892	0.901	0.897	0.890	0.905	0.001	0.000	0.005	0.002	0.001	0.007	0.007
Na	0.025	0.021	0.023	0.025	0.044	0.039	0.030	0.300	0.305	0.302	0.285	0.309	0.294	0.208
K	0.000	0.000	0.000	0.000	0.000	0.000	0.000	1.512	1.553	1.479	1.425	1.516	1.539	1.537
Sum	4.000	4.000	4.000	4.000	4.000	4.000	4.000	15.380	15.438	15.374	15.384	15.419	15.409	15.478
Mg#	90.60	87.79	86.60	86.95	88.03	87.88	92.52	78.23	78.54	77.62	78.95	77.36	78.05	76.35

PM

Table 4. Representative chemical compositions of amphibole and chlorite (in wt%) in the Bayazeh metapicrites and their calculated structural formula (Nosouhian et al., 2014).

Rock Type: Metapicrite

Amphibole — Structural formula based on the 23 equivalent Oxygens

Sample	B460-2	B460-2	B460-2	N11-1	N11-4	N11-4	N11-6
Point	180	188	188	28	43	44	46
Mineral	Act	Tr-Hbl	Tr	Tr	Tr	Tr	Tr
SiO_2	54.38	51.53	58.24	57.88	57.33	57.73	56.19
TiO_2	0.06	0.01	0.02	0.00	0.00	0.01	0.02
Al_2O_3	1.78	3.51	0.00	0.03	0.08	0.24	0.18
Cr_2O_3	0.00	0.00	0.00	0.00	0.00	0.03	0.00
FeO^{total}	8.65	8.78	3.25	4.21	5.40	4.50	4.65
MnO	0.39	0.27	0.12	0.12	0.10	0.09	0.10
MgO	17.71	19.27	22.72	22.09	20.88	21.60	21.73
CaO	15.24	12.65	13.95	13.47	13.23	13.11	13.46
Na_2O	0.73	1.12	0.04	0.03	0.02	0.08	0.07
K_2O	0.05	0.06	0.04	0.04	0.05	0.06	0.07
Total	98.98	97.21	98.37	97.89	97.09	97.42	96.46
Si	7.814	7.284	7.975	7.965	8.001	7.976	7.873
Ti	0.006	0.001	0.002	0.000	0.000	0.001	0.002
$Al^{(IV)}$	0.186	0.584	0.000	0.006	0.000	0.024	0.029
$Al^{(VI)}$	0.114	0.000	0.000	0.000	0.012	0.015	0.000
Cr	0.000	0.000	0.000	0.000	0.000	0.003	0.000
Fe^{2+}	1.039	0.341	0.372	0.408	0.615	0.430	0.398
Fe^{3+}	0.000	0.697	0.000	0.077	0.016	0.090	0.147
Mn	0.047	0.033	0.013	0.014	0.011	0.011	0.011
Mg	3.792	4.061	4.637	4.531	4.344	4.450	4.540
Ca	2.346	1.916	2.047	1.986	1.978	1.941	2.021
Na	0.204	0.308	0.010	0.009	0.005	0.022	0.020
K	0.009	0.011	0.006	0.007	0.008	0.010	0.012
Sum	15.559	15.235	15.063	15.002	14.992	14.973	15.052
Mg#	78.49	92.25	92.57	91.74	87.60	91.19	91.94

Chlorite — Structural formula based on the 28 equivalent Oxygens

Sample	B460-3	N11	N11-2	N11-2
Point	190	199	36	38
Mineral	Clinochlore	Diabantite	Penninite	Penninite
SiO_2	30.21	32.14	33.34	33.66
TiO_2	0.00	0.00	0.02	0.01
Al_2O_3	18.20	15.79	15.50	13.18
Cr_2O_3	0.00	0.00	0.00	0.00
FeO^{total}	9.06	14.77	7.91	8.76
MnO	0.13	0.33	0.19	0.14
MgO	27.35	24.43	29.42	29.95
CaO	0.13	0.05	0.46	0.07
Na_2O	0.00	0.02	0.00	0.01
K_2O	0.01	0.02	0.02	0.08
Total	85.07	87.55	86.85	85.84
Si	5.991	6.368	6.426	6.598
Ti	0.000	0.000	0.003	0.001
$Al^{(IV)}$	2.009	1.632	1.574	1.402
$Al^{(VI)}$	2.241	2.052	1.945	1.639
Cr	0.000	0.000	0.000	0.000
Fe^{2+}	1.502	2.448	1.276	1.436
Fe^{3+}	0.000	0.000	0.000	0.000
Mn	0.021	0.056	0.031	0.023
Mg	8.085	7.214	8.454	8.751
Ca	0.027	0.011	0.095	0.014
Na	0.000	0.006	0.000	0.004
K	0.003	0.005	0.004	0.020
Sum	19.879	19.792	19.808	19.888
Mg#	84.33	74.66	86.89	85.90

Table 5. Representative chemical compositions of serpentine and opaque minerals (in wt%) in the Bayazeh metapicrite and their calculated structural formula (Nosouhian et al., 2014).

Rock Type				Metapicrite				
Sample	N11-1	N11-1	N11-1	Sample	B460-2	B460-2	B460-2	N11-6	N11-6
Point	30	31	35	Point	181	182	187	47	48
Mineral	Srp	Srp	Srp	Mineral	Mag	Ilm	Ilm	Ilm	Ilm
SiO_2	40.39	45.95	42.18	SiO_2	0.20	0.00	0.00	0.00	0.00
TiO_2	0.01	0.03	0.02	TiO_2	0.03	48.73	48.86	49.24	49.28
Al_2O_3	4.56	1.47	3.29	Al_2O_3	0.02	0.01	0.03	0.04	0.03
Cr_2O_3	0.00	0.00	0.02	Cr_2O_3	0.00	1.21	0.52	0.93	0.65
FeO^{total}	8.51	7.52	9.13	FeO^{total}	92.39	43.36	43.78	43.19	42.21
MnO	0.11	0.22	0.29	MnO	0.06	5.22	4.98	4.98	5.32
MgO	32.72	30.05	31.04	MgO	0.10	0.38	0.50	0.44	0.31
CaO	0.28	3.18	0.28	CaO	0.01	0.00	0.01	0.01	0.08
Na_2O	0.06	0.04	0.06	Na_2O	0.02	0.00	0.00	0.01	0.00
K_2O	0.11	0.04	0.10	K_2O	0.00	0.00	0.00	0.00	0.00
Total	86.75	88.49	86.41	Total	92.83	98.91	98.68	98.84	97.88
Oxygen#	7	7	7	Oxygen#	4	3	3	3	3
Si	1.946	2.155	2.039	Si	0.008	0.000	0.000	0.000	0.000
Ti	0.000	0.001	0.001	Ti	0.001	0.941	0.938	0.948	0.957
$Al^{(IV)}$	0.259	0.081	0.187	$Al^{(IV)}$	0.000	0.000	0.000	0.000	0.000
$Al^{(VI)}$	0.000	0.000	0.000	$Al^{(VI)}$	0.001	0.000	0.001	0.001	0.001
Cr	0.000	0.000	0.000	Cr	0.000	0.000	0.000	0.000	0.000
Fe^{2+}	0.343	0.295	0.369	Fe^{2+}	0.998	0.813	0.811	0.822	0.826
Fe^{3+}	0.000	0.000	0.000	Fe^{3+}	1.983	0.118	0.123	0.103	0.085
Mn	0.005	0.009	0.012	Mn	0.002	0.113	0.108	0.108	0.116
Mg	2.351	2.100	2.237	Mg	0.006	0.015	0.019	0.017	0.012
Ca	0.014	0.160	0.015	Ca	0.000	0.000	0.000	0.000	0.002
Na	0.005	0.003	0.006	Na	0.001	0.000	0.000	0.000	0.000
K	0.007	0.002	0.006	K	0.000	0.000	0.000	0.000	0.000
Sum	4.930	4.806	4.872	Sum	3.000	2.000	2.000	1.999	1.999
Mg#	87.27	87.68	85.84						

98.50) (Table 6). The chromian spinels are the large euhedral to subhedral crystals with well-preserved red cores, and partly altered into Fe-rich dark spinel along the fractures and rims (Nosouhian et al., 2016b; Figure 5 E,F). The studied chromian spinel cores have Cr#, Al_2O_3 and TiO_2 values of 60.67-67.59, 16.93-21.41 (wt%) and 0.03-0.09 (wt%), respectively (Table 7). Accordingly, they are Al-, Cr- rich and lie along the Cr-Al join in the Al-Cr-Fe^{3+} ternary diagram (Nosouhian et al., 2016b; Figure 6D).

Amphibole-bearing listwaenite

The Bayazeh amphibole-bearing listwaenites with yellow to brown colour are mainly exposed as massive,

lens shaped veins and veinlets along the shear and/or fault zones in the serpentinites (Figure 4C). These rocks occur as hard and rigid outcrops, more resistant to erosion relative to the surrounding serpentinites (Figure 4C). Field observations support the lineation and foliation of these rocks. The crystallographic orientation of amphiboles in the hand specimen demonstrates the obvious lineation in metalistwaenites. According to the microscopic study (Nosouhian et al., 2016b), the main textures of these rocks are nematoblastic and granoblastic (Figure 5 G,H). The Bayazeh metalistwaenites consist of amphibole, carbonate (dolomite and calcite), quartz and serpentine as major minerals, and chromian spinel, ferritchromite,
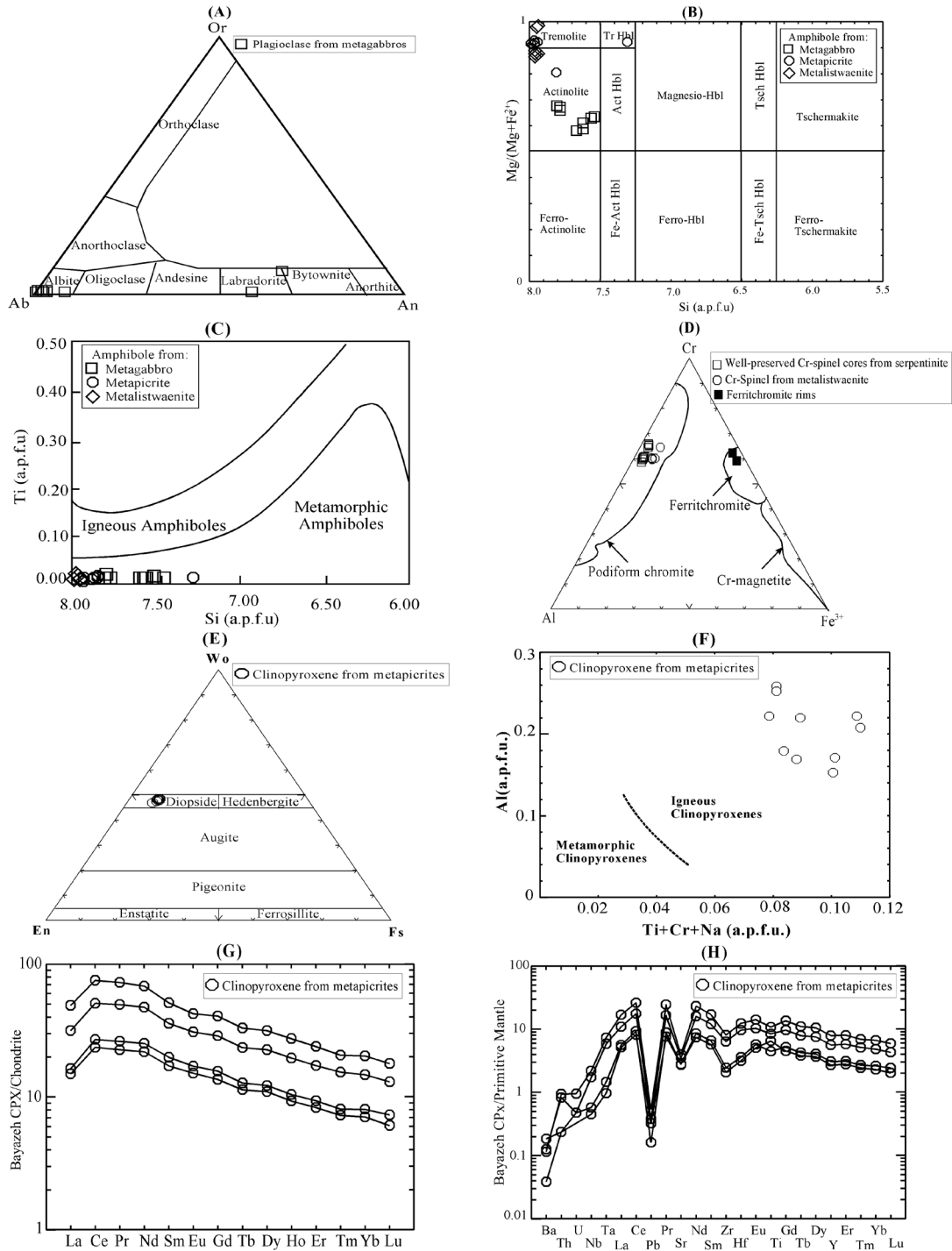
Figure 6. Chemical diagrams of minerals from the Bayazeh ophiolite rock units. A) Feldspar classification triangle in the studied metagabbros (Deer et al., 1992). B) Amphibole classification graph (Deer et al., 1992). C) Amphibole types and position of amphiboles in the studied rock units. Fields are taken from Veblen and Ribbe (1982). D) Chromian spinel composition of the serpentinite and amphibole-bearing listwaenite in Al-Cr-Fe^{3+} triangle. Fields are from Barnes and Roeder (2001). E) Clinopyroxene classification triangle in the studied metapicrites (Morimoto, 1989). F) Clinopyroxene compositions from the metapicrites. The compositional gap between igneous and metamorphic pyroxene has been defined by Berger et al. (2005). G) Chondrite-normalized REE patterns of clinopyroxenes from the metapicrites (Nosouhian et al., 2014). The REE values of chondrite are taken from Sun and McDonough (1989). H) Primitive mantle-normalized multi-element spidergram of clinopyroxenes from the studied metapicrites (Nosouhian et al., 2014). Values of elements in the primitive mantle are taken from McDonough and Sun (1995).

Table 6. Representative chemical compositions of serpentine (in wt%) in the Bayazeh serpentinites and their calculated structural formula (Nosouhian et al., 2016b).

Rock Type	Serpentinite			
Sample	H47	H52	H53	H53
Point	8	50	6	7
Mineral	Srp	Srp	Srp	Srp
SiO$_2$	44.27	47.21	43.90	44.11
TiO$_2$	0.02	0.00	0.00	0.00
Al$_2$O$_3$	0.34	0.21	0.48	0.41
Cr$_2$O$_3$	0.00	0.05	0.36	0.22
FeO^{total}	1.29	1.12	1.09	1.15
MnO	0.04	0.05	0.05	0.00
MgO	41.36	38.38	40.86	40.83
CaO	0.00	0.09	0.00	0.01
Na$_2$O	0.01	0.00	0.00	0.01
K$_2$O	0.00	0.02	0.00	0.00
Total	87.33	87.14	86.74	86.74
Structural formula based on 7 equivalent Oxygens				
Si	2.039	2.158	2.042	2.048
Ti	0.001	0.000	0.000	0.000
Al$^{(IV)}$	0.019	0.011	0.026	0.023
Al$^{(VI)}$	0.000	0.000	0.000	0.000
Cr	0.000	0.000	0.000	0.000
Fe^{2+}	0.050	0.043	0.042	0.045
Fe^{3+}	0.000	0.000	0.000	0.000
Mn	0.002	0.002	0.002	0.000
Mg	2.840	2.616	2.833	2.825
Ca	0.000	0.004	0.000	0.000
Na	0.001	0.000	0.000	0.001
K	0.000	0.001	0.000	0.000
Sum	4.952	4.835	4.945	4.942
Mg#	98.30	98.40	98.50	98.40

chlorite, malachite and azurite as minor minerals (Table 11, Figure 5 G,H). Amphiboles are the main mineral in these rocks (Figure 5H). They define the nematoblastic texture and partly altered to chlorite and magnetite. The chromian spinels are euhedral to subhedral and exhibit well-preserved cores and altered rims. The margins of some chromian spinels are replaced by chlorite (Figure 5 G,H). The presence of chromian spinel and serpentine in the metalistwaenites indicates that their protolith should have been an ultramafic rock (Nosouhian et al., 2016b). The transitional change of serpentinite to metalistwaenite in the field study supports this idea.

The mineral chemistry of amphiboles indicates low contents of TiO$_2$ (<0.09 wt%) and Al$_2$O$_3$ (<1.02 wt%), and high values of Mg# (81.85-97.88) (Nosouhian et al., 2016b; Table 8). They are tremolite and actinolite in composition (Figure 6B, Deer et al., 1992) and all of them represent the metamorphic nature (Figure 6C, Veblen and Ribbe, 1982). Based on the microprobe analyses, Cr#, Al$_2$O$_3$ and TiO$_2$ values of chromian spinel cores range between 64.06 to 69.67, 13.40 to 16.27 (wt%) and 0.31 to 0.73 (wt%), respectively (Table 7). The composition of chromian spinel cores in the Al-Cr-Fe^{3+} ternary diagram lies along the Cr-Al join, whereas the chromian spinel rims with metamorphic origin (ferritchromite) are Al-poor (0.46-0.47) and Fe^{3+}-rich (4.80-5.23) and lie close to the Cr-Fe^{3+} join (Table 7, Figure 6D). The chlorite in the margins of altered chromian spinels is pycnochlorite in composition (Hey, 1954), with 16.34 to 16.89 (wt%) Al$_2$O$_3$ and 2.78 to 3.17 (wt%) Cr$_2$O$_3$ (Table 8). Based on the XRD analyses, the serpentine polytype is as antigorite (Nosouhian et al., 2016b). The microprobe analyses and XRD patterns show that carbonate minerals are dolomite and calcite (Table 8).

WHOLE ROCK GEOCHEMISTRY

The geochemical analyses of the Bayazeh metagabbros show that the SiO$_2$ and MgO contents vary from 47.30 to 51.40 wt% and 3.53 to 11.20 wt%, respectively (Table 9). These characteristics confirm the basic composition of the studied rocks. The Bayazeh metagabbros have contents of 10.90-17.00 (wt%) Al$_2$O$_3$ and 0.16-1.31 (wt%) TiO$_2$ (Table 9). The variation in CaO value (3.09-12.20 wt%) is large. The K$_2$O and Na$_2$O contents of the analyzed rocks are 0.12 to 0.75 wt% and 2.60 to 7.10 wt%, respectively (Table 9). The studied metagabbros have very low content of K$_2$O, which may be explained by the cumulate nature of these rocks. The variations in Na$_2$O contents suggest the effect of sub-sea floor metamorphism in the studied rocks. The loss on ignition (LOI) values of these rocks is 2.60 to 8.61 wt% (Table 9), due to the presence of hydrous minerals and hydrothermal alteration. Field observation, petrographical study and geochemical feature of the Bayazeh mafic rocks indicate differentiation of gabbroic magma and generation of dioritic rocks. According to the whole rock analyses of the metadioritic rocks, these samples have higher SiO$_2$ (52.40-54.70 wt%) and lower CaO (2.50-6.69 wt%) than the metagabbros, but the values of other major elements of these rocks are nearly similar to the metagabbros.

Chondrite-normalized REE patterns of the Bayazeh metagabbros and metadiorites indicate that they are 2 to 15 times and 10 to 30 times more enriched in REE compared to chondrite, respectively (Figure 7A). The studied metagabbros and metadiorites are characterized

Table 7. Representative chemical compositions (in wt%) of chromian spinel cores and metamorphic spinel rims in the Bayazeh serpentinite and metalistwaenite and their calculated structural formula (Nosouhian et al., 2016b).

Rock Type	Serpentinite									Metalistwaenite						
Sample	H47	H47	H47	H47	H47	H52	H52	H52	H52	H56	H56	H56	H56	H56	H56-1	H56-1
Point	41	42	44	45	46	47	48	51	52	248	249	250	253	259	52	55
Mineral	Cr-Spl	Cr-Spl	Cr-Spl	Cr-Spl	Cr-Spl	Cr-Spl	Cr-Spl	Cr-Spl	Cr-Spl	Cr-Spl	Cr-Spl	Cr-Spl	Cr-Spl	Cr-Spl	Ferritchromite	Ferritchromite
Analysis	Core									Core					Rim	
SiO_2	0.02	0.02	0.18	0.00	0.00	0.10	0.01	0.00	0.15	0.00	0.01	0.03	0.00	0.01	0.68	0.23
TiO_2	0.04	0.03	0.03	0.07	0.03	0.09	0.07	0.07	0.08	0.34	0.31	0.33	0.60	0.73	0.03	0.06
Al_2O_3	21.41	20.28	18.97	20.01	20.69	16.97	16.29	17.59	16.93	15.89	16.27	16.21	13.40	16.14	1.25	1.22
Cr_2O_3	49.24	49.67	49.75	50.07	49.71	52.75	52.60	51.62	52.10	44.10	43.67	43.74	45.91	42.90	39.28	41.41
FeO^{total}	16.55	16.62	16.29	16.32	16.56	17.98	18.91	20.32	18.58	36.53	37.20	37.31	37.67	37.93	53.12	50.79
MnO	0.10	0.17	0.21	0.21	0.22	0.32	0.26	0.36	0.37	1.04	1.42	1.40	1.55	1.45	1.31	1.53
MgO	14.61	14.03	14.61	14.28	14.27	12.19	12.10	11.06	11.85	1.87	0.68	0.47	0.39	0.40	0.10	0.08
CaO	0.00	0.00	0.00	0.00	0.00	0.01	0.00	0.01	0.01	0.01	0.01	0.01	0.00	0.00	0.01	0.02
Na_2O	0.00	0.01	0.00	0.00	0.02	0.00	0.03	0.03	0.03	0.01	0.04	0.04	0.05	0.05	0.09	0.12
K_2O	0.00	0.00	0.00	0.00	0.00	0.00	0.00	0.00	0.00	0.00	0.00	0.00	0.00	0.00	0.00	0.01
Total	101.97	100.83	100.04	100.96	100.50	100.41	100.27	101.07	100.10	99.79	99.61	99.54	99.57	99.61	95.87	95.47
Structural formula based on 32 equivalent Oxygens																
Si	0.005	0.004	0.043	0.000	0.000	0.026	0.002	0.000	0.038	0.000	0.001	0.008	0.000	0.002	0.220	0.073
Ti	0.007	0.006	0.005	0.013	0.006	0.018	0.014	0.014	0.016	0.072	0.065	0.068	0.126	0.153	0.007	0.015
Al	6.069	5.849	5.690	5.758	5.914	5.038	5.092	5.219	5.055	5.134	5.302	5.297	4.438	5.273	0.472	0.461
Cr	9.361	9.607	9.698	9.664	9.530	10.506	10.391	10.272	10.433	9.556	9.545	9.583	10.195	9.400	9.984	10.528
Fe^{2+}	2.758	2.864	2.709	2.779	2.813	3.385	3.458	3.794	3.483	7.047	7.430	7.526	7.581	7.614	8.400	8.176
Fe^{3+}	0.549	0.516	0.570	0.533	0.525	0.393	0.471	0.462	0.444	1.195	1.051	1.011	1.139	1.054	5.236	4.803
Mn	0.020	0.036	0.043	0.043	0.045	0.069	0.056	0.077	0.079	0.241	0.332	0.328	0.369	0.342	0.357	0.417
Mg	5.237	5.118	5.263	5.198	5.160	4.578	4.509	4.150	4.474	0.765	0.281	0.194	0.165	0.164	0.046	0.041
Ca	0.000	0.000	0.000	0.000	0.000	0.000	0.000	0.000	0.000	0.000	0.000	0.000	0.000	0.000	0.000	0.000
Na	0.000	0.000	0.000	0.000	0.000	0.000	0.000	0.000	0.000	0.000	0.000	0.000	0.000	0.000	0.000	0.000
K	0.000	0.000	0.000	0.000	0.000	0.000	0.000	0.000	0.000	0.000	0.000	0.000	0.000	0.000	0.000	0.000
Sum	24.006	23.999	24.021	23.987	23.992	24.012	23.992	23.988	24.021	24.010	24.009	24.014	24.012	24.003	24.722	24.511
Fe^{3+}#	3.43	3.23	3.57	3.34	3.29	2.47	2.95	2.89	2.78	7.52	6.61	6.36	7.22	6.70	33.37	30.41
Mg#	65.51	64.12	66.02	65.17	64.72	57.49	56.59	52.24	56.23	9.79	3.65	2.51	2.12	2.11	0.55	0.50
Cr#	60.67	62.16	63.02	62.66	61.71	67.59	67.11	66.31	67.36	65.05	64.29	64.40	69.67	64.06	95.48	95.81
F%	18.33	18.60	18.77	18.70	18.53	19.65	19.56	19.40	19.60	-	-	-	-	-	-	-

Table 8. Representative chemical compositions of amphibole, chlorite, dolomite and calcite (in wt%) in the Bayazeh metalistwaenites and their calculated structural formula (Nosouhian et al., 2016b).

Rock Type — Metalistwaenite

Sample	H56	H56	H56	H56	H56	H56	H56-1	H56-1	H56-1	H56-1
Point	255	256	258	51	53	54	65	66	67	68
Mineral	Act	Act	Act	Act	Act	Act	Act	Tr	Act	Tr
SiO_2	57.01	57.55	57.27	57.61	57.44	57.33	58.29	57.68	58.00	58.13
TiO_2	0.03	0.01	0.01	0.09	0.03	0.02	0.00	0.04	0.01	0.04
Al_2O_3	1.02	0.74	0.50	0.45	0.73	0.57	0.63	0.16	0.64	0.66
Cr_2O_3	0.32	0.04	0.13	0.10	0.13	0.97	0.41	0.05	0.52	0.12
FeO^{total}	7.88	9.14	9.91	8.35	9.12	7.50	7.05	3.27	7.59	3.46
MnO	0.19	0.17	0.23	0.18	0.15	0.15	0.18	0.08	0.22	0.10
MgO	18.35	17.90	17.85	19.37	18.78	19.36	19.19	22.78	19.65	22.71
CaO	11.44	9.95	10.13	10.62	10.31	11.24	11.74	12.83	10.95	12.87
Na_2O	0.90	1.80	1.66	1.21	1.86	1.27	1.06	0.28	1.53	0.39
K_2O	0.11	0.03	0.02	0.01	0.04	0.03	0.01	0.01	0.03	0.02
Total	96.93	97.29	97.59	97.91	98.47	97.46	98.15	97.13	98.61	98.37

Structural formula based on 23 equivalent Oxygens

	H56	H56	H56	H56	H56	H56	H56-1	H56-1	H56-1	H56-1
Si	8.000	8.000	8.000	7.942	7.929	7.925	8.000	7.974	7.938	7.895
$Al^{(IV)}$	0.000	0.000	0.000	0.058	0.071	0.075	0.000	0.026	0.062	0.105
$Al^{(VI)}$	0.169	0.121	0.083	0.015	0.048	0.018	0.102	0.000	0.042	0.000
Ti	0.003	0.001	0.001	0.009	0.003	0.002	0.000	0.004	0.001	0.004
Cr	0.035	0.004	0.015	0.010	0.014	0.105	0.044	0.006	0.056	0.013
Fe^{2+}	0.852	0.778	0.747	0.412	0.604	0.594	0.815	0.101	0.527	0.130
Fe^{3+}	0.074	0.291	0.411	0.551	0.449	0.273	0.000	0.218	0.341	0.251
Mn	0.022	0.020	0.027	0.021	0.018	0.017	0.021	0.009	0.025	0.011
Mg	3.841	3.733	3.716	3.981	3.864	3.991	3.957	4.662	4.008	4.591
Ca	1.717	1.439	1.516	1.569	1.525	1.665	1.680	1.887	1.606	1.869
Na	0.245	0.489	0.450	0.323	0.498	0.339	0.284	0.073	0.405	0.102
K	0.020	0.006	0.004	0.002	0.006	0.005	0.001	0.002	0.005	0.004
Sum	14.987	14.986	14.971	14.894	15.029	15.009	15.025	14.963	15.016	14.975
Mg#	81.85	82.75	83.26	90.62	86.48	87.04	82.92	97.88	88.38	97.25
Fe^{3+}#	0.08	0.27	0.35	0.57	0.43	0.31	0.00	0.68	0.39	0.66

Metalistwaenite (continued)

Sample	H65	H65	H65	H65	H65
Point	251	252	254	257	69
Mineral	Pyc	Pyc	Pyc	Dol	Cal
SiO_2	29.65	29.39	30.30	0.65	0.02
TiO_2	0.01	0.00	0.00	0.00	0.01
Al_2O_3	16.49	16.89	16.34	0.06	0.00
Cr_2O_3	2.89	3.17	2.78	0.11	0.00
FeO^{total}	16.08	15.88	16.77	4.81	0.24
MnO	0.17	0.11	0.12	0.06	0.31
MgO	21.66	22.43	23.14	16.50	0.31
CaO	0.14	0.06	0.04	31.38	57.42
Na_2O	0.00	0.02	0.02	0.05	0.03
K_2O	0.01	0.01	0.01	0.00	0.00
Total	87.12	87.95	89.52	53.52	58.35
Oxygens	28	28	28	6	6
Si	6.017	5.907	5.997	0.018	0.001
Ti	0.002	0.000	0.000	0.000	0.000
Al	1.983	2.093	2.003	0.002	0.000
Cr	1.959	1.906	1.805	0.000	0.000
Fe^{2+}	0.464	0.502	0.435	0.128	0.007
Fe^{3+}	2.729	2.669	2.776	0.000	0.000
Mn	0.000	0.000	0.000	0.002	0.009
Mg	0.030	0.018	0.019	0.781	0.015
Ca	6.555	6.722	6.828	1.067	1.967
Na	0.031	0.012	0.008	0.003	0.002
K	0.000	0.008	0.006	0.000	0.000
Sum	19.774	19.839	19.880	2.001	2.001
Mg#	71.00	72.00	71.00		
Fe^{2+}#	29.00	28.00	29.00		

PM

Table 9. ICP-MS analyses of the Bayazeh metagabbros (major elements in wt% and trace elements in ppm) (D.L.: Detection Limits).

Rock Type		Metagabbro						Metadiorite		
Sample	D.L.	N12	N13	N16	N23	N28	H25	N14	N18	N19
SiO_2	0.01	47.30	47.50	49.70	50.90	51.40	51.30	53.10	54.70	52.40
TiO_2	0.01	0.25	0.25	0.24	1.18	1.31	0.16	0.60	0.78	0.19
Al_2O_3	0.01	10.90	10.90	17.00	14.00	15.20	15.96	16.00	16.10	17.50
$Fe_2O_3^{total}$	0.01	7.01	7.06	7.05	11.70	11.10	6.49	9.39	10.90	4.84
MnO	0.01	0.16	0.16	0.14	0.10	0.16	0.14	0.13	0.11	0.10
MgO	0.01	11.10	11.20	9.96	3.53	4.97	9.94	7.86	6.14	6.50
CaO	0.01	12.20	12.20	7.71	3.09	8.89	9.39	4.52	2.50	6.69
Na_2O	0.01	2.60	2.60	3.90	7.10	4.20	3.11	2.70	4.10	5.10
K_2O	0.01	0.12	0.12	0.29	0.14	0.75	0.17	0.21	0.09	0.56
P_2O_5	0.01	0.01	0.01	0.02	0.12	0.11	0.00	0.05	0.05	0.01
LOI	0.01	8.58	8.61	3.53	4.24	2.60	2.96	4.93	3.90	2.36
Sum	0.01	100.30	100.80	99.60	96.10	100.70	99.62	99.40	99.30	96.30
Cr	10	753	753	68	68	68	240	68	68	68
Ni	5	104	104	61	16	52	95	29	7	52
Co	0.5	37.1	37.4	35.1	26.1	45.8	38.0	29.3	32.7	21.4
V	5	186	189	146	365	320	141	23	331	109
Cu	5	113	116	76	43	81	49	29	22	20
Zn	5	48	49	39	86	101	61	46	29	65
Rb	0.2	1.7	1.5	3.3	2.5	16.0	2.0	9.1	1.1	5.3
Cs	0.1	0.3	0.2	0.2	1.0	1.1	0.1	1.7	0.1	0.3
Ba	10	30	20	40	1330	60	64	80	30	90
Sr	10	170	170	210	110	270	246	220	110	190
Ta	0.5	0.50	0.50	0.50	0.50	0.50	0.08	0.50	0.50	0.50
Nb	1	1.0	1.0	1.0	1.0	1.0	0.2	1.0	1.0	1.0
Hf	1	1.0	1.0	1.0	2.0	2.0	0.2	1.0	1.0	1.0
Zr	10	10.8	10.9	14.0	72.1	62.5	8.0	39.0	45.9	16.1
Y	0.5	8.2	8.2	6.4	21.4	25.7	5.7	15.1	14.3	6.6
Th	0.1	0.10	0.10	0.20	0.40	0.20	0.06	0.60	0.80	0.30
U	0.05	0.19	0.12	0.12	0.27	0.47	0.07	0.45	0.53	0.16
La	0.1	2.10	3.10	1.60	4.20	3.80	0.60	3.70	6.60	2.60
Ce	0.1	2.80	3.10	2.90	8.50	8.60	1.60	7.10	11.00	3.60
Pr	0.05	0.44	0.44	0.45	1.39	1.51	0.22	1.05	1.50	0.47
Nd	0.1	2.40	2.50	2.10	7.20	8.30	1.10	5.00	7.30	2.30
Sm	0.1	0.90	0.90	0.70	2.30	2.90	0.45	1.70	2.00	0.60
Eu	0.05	0.33	0.33	0.31	0.75	1.07	0.28	0.63	0.71	0.37
Gd	0.05	1.27	1.35	0.94	3.27	3.91	0.73	2.27	2.40	0.94
Tb	0.05	0.24	0.23	0.20	0.63	0.75	0.15	0.44	0.44	0.17
Dy	0.05	1.49	1.50	1.24	4.12	5.04	0.96	2.83	2.88	1.13
Ho	0.05	0.36	0.35	0.26	0.92	1.13	0.22	0.63	0.60	0.27
Er	0.05	0.95	0.92	0.84	2.61	3.25	0.68	1.90	1.71	0.75
Tm	0.05	0.15	0.14	0.13	0.41	0.49	0.10	0.28	0.29	0.11
Yb	0.1	0.90	0.90	0.80	2.70	3.20	0.61	1.80	2.00	0.70
Lu	0.05	0.15	0.16	0.14	0.40	0.47	0.09	0.31	0.33	0.10

PM

by the (La/Yb)$_{CN}$ ratios of 0.81 to 2.43 and 1.40 to 2.52, respectively. These ratios indicate that all samples present a nearly horizontal trend for REEs in the chondrite-normalized diagram, supporting the tholeitic nature of the parental magma. The primitive mantle-normalized multi-element diagram indicates enrichment in LILE (Cs, Ba, K, Sr), relative to HFSE (Nb, Th, Ti) and HREE (Figure 7B).

The Bayazeh analyzed metapicrites have modal contents of olivine and clinopyroxene between 37 to 39 and 33 to 36 vol% respectively, confirming their ultramafic nature. Accordingly, they have SiO$_2$ content of 37.50 to 39.40 wt%, MgO values of 25.80 to 28.00 wt% and Mg# contents varying from 80.61 to 81.60 (Table 10). The Al$_2$O$_3$ and TiO$_2$ amounts are 6.13 to 6.63 wt% and 0.46 to 0.55 wt%, respectively. According to IUGS classification (Le Bas, 2000), these rocks have low values of K$_2$O (0.38-0.45 wt%), Na$_2$O (0.10-0.12 wt%), and CaO (3.56 to 4.42 wt%) (Table 10). The compositions of studied rocks have the high amount of MgO (25.80-28.00

wt%), and low values of SiO$_2$ (37.50-39.40 wt%) and Na$_2$O + K$_2$O (0.48-0.57 wt%) (Table 10). The high value of MgO in the Bayazeh metapicrites does not represent the MgO content of a melt because a large amount of olivine (37-39 vol%) appears as cumulus crystals. Also, the high amounts of Ni (975-1020 ppm) and Cr (1300-1431 ppm) confirm ultramafic nature and can be related to the olivine accumulation in the studied metapicrites. Also, the LOI contents of these rocks are 8.98 to 11.05 wt% (Table 10). The high LOI values are due to the presence of hydrous minerals such as phlogopite, serpentine, amphibole and chlorite, and the result of extensive serpentinization.

The studied metapicrites indicate parallel patterns in both chondrite and primitive mantle-normalized diagrams, implying that they were derived from a similar source (Nosouhian et al., 1014; Figure 7 C,D). Chondrite-normalized REE patterns of the metapicrites show that they are 3 to 50 times more enriched in REE compared to chondrite (Figure 7C). In this diagram, all samples
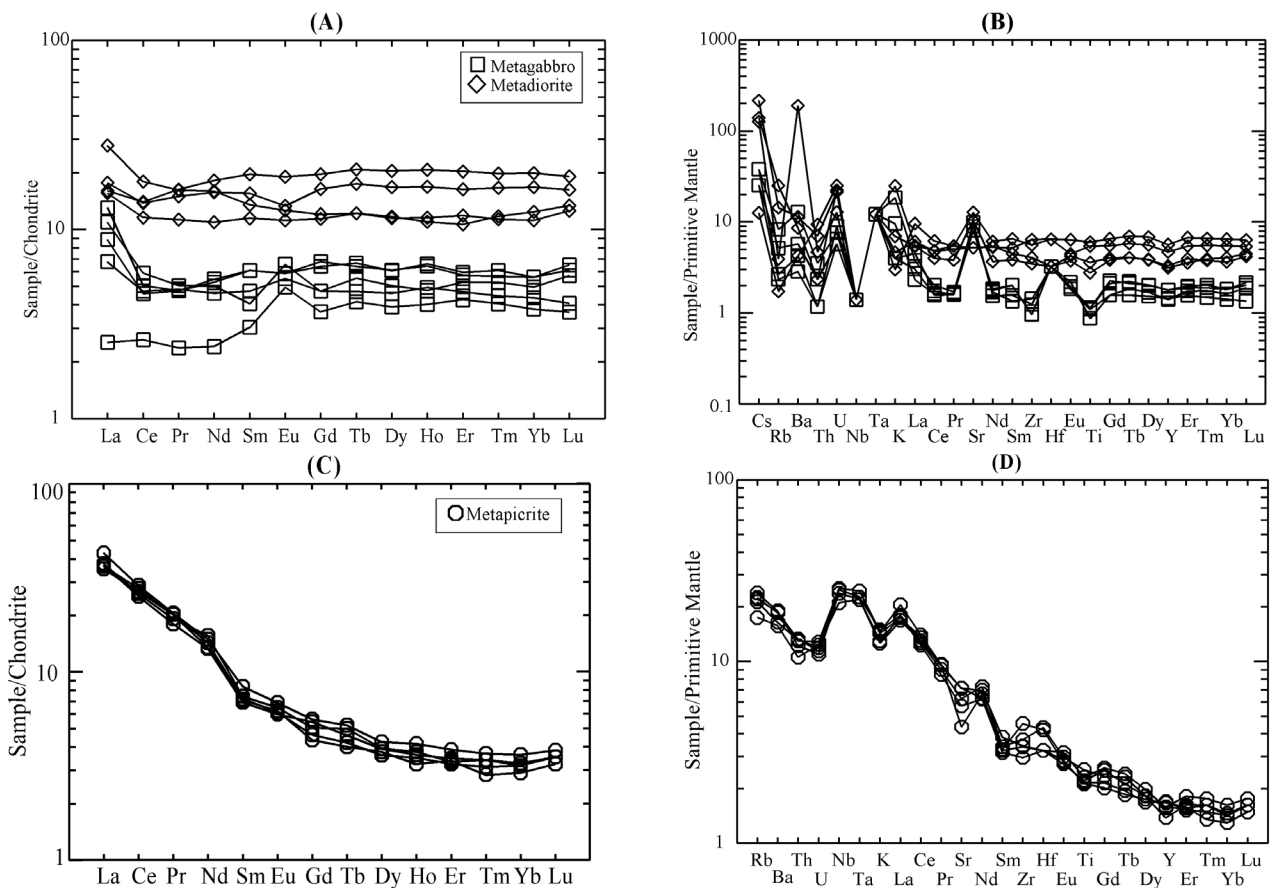

Figure 7. Geochemical diagrams of whole rock samples from the Bayazeh ophiolite rock units; A,B) Chondrite-normalized REE patterns and primitive mantle-normalized spidergram from the studied metagabbro. C,D) Chondrite-normalized REE patterns and primitive mantle-normalized variation diagram from the Bayazeh metapicrite (Nosouhian et al., 2014). Normalizing values of chondrite and primitive mantle are taken from Sun and McDonough (1989), and McDonough and Sun (1995), respectively.

Table 10. LA-ICP-MS analyses of clinopyroxenes (left part) and ICP-MS analyses of the Bayazeh metapicrites (right part) (major elements in wt% and trace elements in ppm) (D.L.: Detection Limits) (Nosouhian et al., 2014).

Rock Type				Metapicrite						
	LA-ICP-MS: Cpx of metapicrite			ICP-MS: Whole rock data						
Sample /Point	N11-1/27	N11-2/39	B460-2/183	Sample	D.L.	N10	N11	B460	B650	B651
SiO_2	51.62	49.33	50.41	SiO_2	0.01	38.00	37.50	39.40	38.40	38.95
TiO_2	0.97	1.40	1.83	TiO_2	0.01	0.48	0.50	0.47	0.46	0.55
Al_2O_3	3.61	5.22	3.66	Al_2O_3	0.01	6.63	6.61	6.13	6.24	6.49
Cr_2O_3	0.64	0.86	0.10	$Fe_2O_3^{total}$	0.01	12.50	12.30	12.25	12.70	12.80
FeO^{total}	4.52	5.00	5.16	MnO	0.01	0.18	0.19	0.17	0.18	0.20
MnO	0.12	0.11	0.11	MgO	0.01	28.00	27.20	25.80	27.60	26.87
MgO	15.85	14.69	14.92	CaO	0.01	3.56	4.21	3.58	4.42	4.33
CaO	22.68	22.49	23.55	Na_2O	0.01	0.10	0.10	0.11	0.10	0.12
Na_2O	0.34	0.37	0.68	K_2O	0.01	0.39	0.44	0.43	0.38	0.45
K_2O	0.00	0.00	0.00	P_2O_5	0.01	0.20	0.21	0.26	0.21	0.20
NiO	0.02	0.04	0.03	LOI	0.01	10.10	8.98	11.05	10.15	9.14
Total	100.37	99.51	100.46	Total	0.01	100.20	98.30	99.90	101.00	100.10
Pb	0.03	0.06	0.07	Cr	10	1300	1300	1380	1420	1431
Rb	0.02	0.01	0.05	Ni	5	975	1020	1010	1010	994
Ba	0.27	1.29	0.88	Co	0.5	97.5	103.0	110.5	113.5	107.5
Sr	58.74	58.03	74.49	V	5	85	100	100	93	91
Li	2.32	3.38	5.80	Cu	5	79	49	26	29	39
Ta	0.06	0.04	0.24	Zn	5	114	64	76	73	79
Nb	0.41	0.32	1.24	Rb	0.2	11.1	14.3	14.0	15.1	13.5
Hf	1.11	0.97	2.98	Cs	0.1	16.7	21.7	20.9	14.2	18.2
Zr	27.52	23.21	71.23	Ba	10	110	130	131	133	115
Y	14.03	12.27	25.56	Sr	10	120	150	92	151	132
Th	0.02	0.02	0.07	Ta	0.5	0.9	1.0	1.0	0.9	0.9
U	0.01	0.00	0.01	Nb	1	15.0	18.0	18.0	17.0	17.6
La	3.87	3.54	7.49	Hf	1	1.0	1.0	1.3	1.0	1.3
Ce	16.55	14.44	31.07	Zr	10	40	50	51	38	42
Pr	2.44	2.10	4.60	Y	0.5	6.3	7.2	7.7	7.6	7.1
Nd	11.54	10.01	21.66	Th	0.1	0.9	1.1	1.1	1.0	1.1
Sm	2.94	2.54	5.29	U	0.05	0.26	0.27	0.24	0.23	0.25
Eu	0.96	0.85	1.74	La	0.1	12.2	14.1	12.0	11.6	12.4
Gd	3.11	2.70	5.75	Ce	0.1	21.9	24.9	24.1	23.2	22.6
Tb	0.46	0.41	0.85	Pr	0.05	2.34	2.67	2.66	2.63	2.50
Dy	3.00	2.70	5.58	Nd	0.1	8.4	9.4	9.0	8.5	9.9
Ho	0.57	0.51	1.07	Sm	0.1	1.4	1.7	1.5	1.4	1.5
Er	1.50	1.33	2.76	Eu	0.05	0.46	0.53	0.47	0.48	0.50
Tm	0.20	0.18	0.38	Gd	0.05	1.50	1.55	1.28	1.20	1.39
Yb	1.30	1.14	2.37	Tb	0.05	0.23	0.26	0.21	0.20	0.25
Lu	0.18	0.15	0.32	Dy	0.05	1.34	1.46	1.24	1.29	1.35
Mg#	0.778	0.746	0.743	Ho	0.05	0.28	0.32	0.27	0.25	0.20
				Er	0.05	0.78	0.87	0.73	0.76	0.75
				Tm	0.05	0.12	0.13	0.11	0.10	0.12
				Yb	0.1	0.7	0.8	0.7	0.6	0.7
				Lu	0.05	0.12	0.13	0.12	0.11	0.12

PM

Table 11. Summary of rock-forming minerals, textures and hydrothermal alterations in the Bayazeh ophiolite litological units.

	Rock type	Metagabbro	Metapicrite	Serpentinite	Metalistwaenite
Stage of crystallization	Magmatic	Plagioclase (Lab)	Clinopyroxene (Di), Phlogopite	Cr-spinel	Cr-spinel
	Metamorphic	Amphibole (Act)	Serpentine (Atg), Amphibole (Tr, Act, Tr-Hbl)	Serpentine (Atg), Amphibole (Tr, Act)	Amphibole (Tr, Act), Serpentine (Atg), Ferritchromite
	Alteration	Actinolite, Albite, Calcite, Quartz Epidote, Chlorite, Magnetite, Titanite	Amphibole, Prehnite, Chlorite, Ilmenite, Magnetite, Apatite	Magnetite, Chlorite	Dolomite, Calcite Quartz, Chlorite Magnetite
Texture		Granoblastic, Nematoblastic, Poikiloblastic	Porphyroblastic, Poikiloblastic	Mesh texture	Nematoblastic, Granoblastic,
Hydrothermal alteration		Sub-sea-floor metamorphism, Securitization, Albitization, Chloritization	Serpentinization, Chloritization, Prehnitization, Devitrification	Serpentinization	Listwaenitization, Chloritization

are enriched in LREE relative to HREE with $(La/Yb)_{CN}$ ratios of 11.65 to 12.31. The primitive mantle-normalized spider diagram indicates enrichment in LILE, relative to HFSE and HREE (Figure 7D). The negative K and Ti, and positive Cs, Ta and Nb anomalies are present in the trace element patterns of these rocks (Figure 7D).

Field observations and petrographic study of the Bayazeh rock units show that these rocks have been affected by alteration and upper greenschist to lower amphibolite facies metamorphism. The considerably high LOI values in the analyzed rocks are due to the presence of hydrous (primary or metamorphic) minerals and the effects of hydrothermal alteration. Despite the effect of alteration and metamorphism in the studied rocks, the distribution of immobile major elements such as Al and Ti, and most of the HFSE and REE is regular, which suggests that they have not undergone significant changes.

DISCUSSION
Petrogenesis of the Bayazeh peridotite

Peridotites of the Bayazeh ophiolite have been completely replaced by serpentinite. Serpentinites are commonly distributed in this ophiolite. The relicts of well-preserved chromian spinel cores with magmatic natures in serpentinites are used as a petrogenetic indicator for highly altered rocks where the chromian spinels are often the only discriminating mineral (e.g. Arai et al., 2011; Pomonis and Magganas, 2017). The chemical composition of chromian spinel cores in the Bayazeh serpentinites indicates the high Cr and Mg values, and low Fe^{3+} and Ti contents, supporting their primary nature (Table 7). They lie along the Cr-Al join in the $Cr-Al-Fe^{3+}$ ternary diagram, indicating magmatic origin of the chromian spinel cores (Figure 6D). Accordingly, the studied chromian spinels

represent the chemical composition of mantle chromites and confirm an ophiolitic origin (Figure 8A). The low TiO_2 contents in these minerals point to an origin from a depleted mantle source (Jan and Windley, 1990; Farahat, 2008). The low value of Fe^{3+} (0.39-0.57) and low ratio of Fe^{3+}/Fe^{2+} (0.12-0.20) in the investigated chromian spinel cores show the reduced nature of their primary source (Pal and Mitra, 2004). The Cr# of the studied chromian spinel cores ranges from 60.67 to 67.59 (Table 7), reflecting a harzburgite or dunite as the protolith. The high amount of bastite in the serpentinites indicates that the predominant protolith should have been a harzburgite.

The Cr# of chromian spinels in a mantle peridotite is a good tool for estimation of degree of partial melting (Dick and Bullen, 1984; Arai, 1994; Hellebrand et al., 2001). Hellebrand et al. (2001) have applied the Cr# ratio in the spinel equation $[F\%=10ln(Cr/Cr+Al)_{spinel}]$ for the calculation of the degree of partial melting. Based on the mineral chemistry of chromian spinel cores in the serpentinite (Table 7), the estimated degree of partial melting for peridotites in the Bayazeh ophiolite is ranging from 18.33% to 19.65% (Nosouhian et al., 2016b).

The geotectonic setting of the host peridotite can be inferred from the chemical composition of chromian spinels (e.g., Kamenetsky et al., 2001; Arai et al., 2011). Tectonic discrimination diagrams such as Al_2O_3 versus TiO_2 diagram show that the studied well-preserved chromian spinels belong to the supra-subduction zone peridotites (Nosouhian et al., 2016b; Figure 8B). The geological and geotectonic history of CEIM confirm a SSZ (back-arc) setting for the metamorphosed ophiolitic mélange with Paleozoic age in the Yazd block (Bagheri, 2007; Bagheri and Stampfli, 2008; Torabi and Arai, 2013).
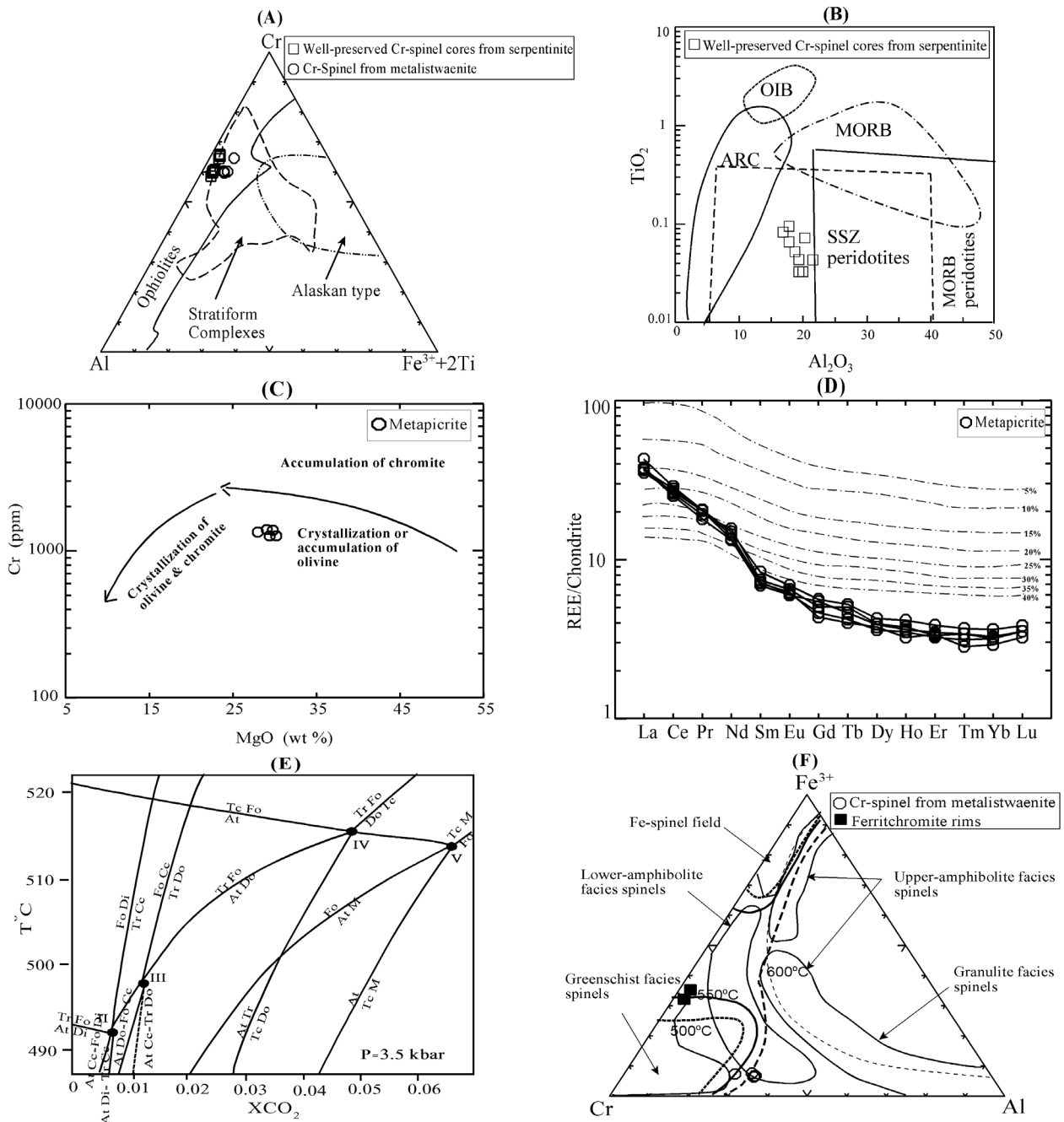
Figure 8. A) Composition of chromian spinel in Al-Cr-(Fe^{3+}+2Ti) graph for the studied serpentinite and amphibole-bearing listwaenite. Fields are taken from Jan and Windley (1990) (Nosouhian et al., 2016b). B) Al$_2$O$_3$ versus TiO$_2$ tectonic discrimination diagram based on the investigated chromian spinel in the serpentinite. Fields are from Kamenetsky et al. (2001) (Nosouhian et al., 2016b). C) Cr versus MgO diagram from the studied metapicrite. Fields are from Arndt (2008) (Nosouhian et al., 2014). D) REE compositions of modeled melts at 5% melting increments obtained by partial melting of spinel peridotite source composed of a 57:25.5:15:2.5 mixture of olivine:orthopyroxene:clinopyroxene:spinel. A mantle composition was based on a 2:1 ratio mixture of primitive (McDonough and Frey, 1989) to sub-continental mantle (McDonough, 1990) (Nosouhian et al., 2014). E) T-XCO$_2$ diagram for the amphibole-bearing listwaenite in the CaO-MgO-SiO$_2$-CO$_2$-H$_2$O system from Trommsdorff and Evans (1974; 1977). According to the mineral assemblages, the dashed line indicates the metamorphism condition of the studied amphibole-bearing listwaenite (Nosouhian et al., 2016b). F) Studied chromian spinel and ferritchromite from the amphibole-bearing listwaenite plotted in Cr-Fe^{3+}-Al triangular diagram. Fields are taken from Barnes and Roeder (2001), Evans and Frost (1975), Suita and Strieder (1996) and solvus determined at 500, 550 and 600 °C by Sack and Ghiorso (1991).

Petrogenesis of the Bayazeh metagabbro

Petrography and mineral chemistry of the Bayazeh metagabbros show that they are affected by the sub-solidus evolutions such as sub-sea floor metamorphism, hydrothermal alteration and regional metamorphism. According to the hydrothermal circulation effects, the primary minerals of gabbros are changed and the fresh plagioclase and amphibole are not present (Figure 5 A,B). The geochemical characteristics of the Bayazeh metagabbros indicate the high variation in Na_2O (2.60-7.10 wt%) and CaO (3.09-12.20 wt%) contents (Table 9). The variations in Na_2O values suggest the effect of sub-sea floor metamorphism that changed the primary calcic plagioclase to secondary sodic ones. Also, the variations of CaO content are resulted by variation in modal content of plagioclase, amphibole and epidote. The studied metagabbros have very low content of K_2O (0.12-0.75 wt%), which may be explained by the cumulate nature of these rocks. The value of Al_2O_3 (10.90-17.00 wt%) has anticorrelates with MgO (3.53-11.20 wt%) and $Fe_2O_3^*$ (6.49-11.70 wt%) indicating the relative abundance of plagioclase versus other minerals in the Bayazeh metagabbro. Also, the SiO_2 (47.30-51.40 wt%) content have anticorrelates with Al_2O_3 (10.90-17.00 wt%) and CaO (3.09-12.20 wt%) abundances, most likely reflecting the calcic nature of the plagioclase in the cumulus metagabbros.

The chondrite-normalized REE patterns of the Bayazeh metagabbros and metadiorites show a nearly horizontal trend (Figure 7A), which are characterized by the (La/Yb)$_{CN}$ ratios of 0.81 to 2.43 and 1.40 to 2.52, respectively. The enrichment of metadiorites compared to metagabbros in the chondrite-normalized diagram, indicates that metadiorites are generated by differentiation of gabbroic magma (Figure 7A). The metagabbros have positive Eu anomaly, indicating Eu/Eu* ratios (Eu/Eu*=Eu$_{CN}$/(Sm$_{CN}$ * Gd$_{CN}$)$^{0.5}$; McLennan and Taylor, 1991) ranges from 0.83 to 1.17. REE patterns of the Bayazeh metagabbros are flat at the chondrite-normalized diagram with small positive anomaly of Eu (0.83-1.17). The positive Eu anomalies can be attributed to Eu in the cumulus plagioclase.

The enrichment in LILE relative to HFSE and HREE are evident in the primitive mantle-normalized multi-element diagram of metagabbros (Figure 7B). Positive anomalies of Cs, Ba, K and Sr and negative spikes of Nb, Th and Ti are obvious in the primitive mantle-normalized multi-element diagram of metagabbros (Figure 7B). Low values of HFSE in the studied gabbros reveals important role of lithospheric mantle in the generation of the Bayazeh gabbros. According to the Abdel-Fattah et al. (2004), the high Nb/La ratio (>1) and low Nb/La ratio (<0.5) of basalts indicate that they are derived from an asthenospheric mantle source and a lithospheric mantle

source, respectively. Therefore, the low ratios of Nb/La (0.24-0.63) of the metagabbros support that these rocks were generated from the lithospheric mantle. The value of Sm/Yb ratio depends on the proportion of garnet and it may be used to determine the source mineralogy, since Yb is compatible in garnet (Alici Sen et al., 2004). Low Sm/Yb ratios (0.74-1.00) and low amount of Yb in the Bayazeh metagabbros suggest that garnet was absent in the melting source. Furthermore, the nearly horizontal trend of the HREE, low degree of HREE fraction [(Gd/Yb)$_{CN}$=0.95-1.21] and low degree of REE differentiation ((La/Yb)$_{CN}$=0.81-2.43) are indicative of the spinel lherzolite facies of mantle as a suitable source for generation of this magma (e.g. Shkoľnik et al., 2011).

The Bayazeh metagabbros reveal enrichment in the LILE and U relative to HFSE. These characteristic suggesting the protolith is a cumulate gabbro rather than a noncumulate (isotropic) gabbro. The enrichment of LILE compared to HFSE and depletion of Nb and Ti relative to other HFSE indicate involvement of subduction component in the depleted mantle source, and suggest that these rocks were formed in a subduction zone (e.g. Arndt, 2008). The negative Ti anomaly in the primitive mantle-normalized diagram (Figure 7B) may be related to residual titanium phases such as rutile and ilmenite in the subduction-related magmas (Stalder et al., 1998). The enrichment in Cs relative to Rb in the spidergram can be attributed to mantle metasomatism. Accordingly, the relatively large variation of the LILE/HFSE ratios in the studied rocks (Figure 7B) can be ascribed to addition of a subduction fluid to the mantle source (e.g. Tonarini et al., 2001).

Chemical characteristics of the studied metagabbros, such as their high Zr/Nb (10.80-72.10) and low Zr/Y ratios (1.31-3.37) (Table 9), indicate that the parental magma was generated by a high degree partial melting of a mantle source (e.g. Tsikouras et al., 2008). Therefore, high degree partial melting of lithospheric mantle that was previously enriched in incompatible elements is considered as the most likely explanation for the origin of the magmas generated the Bayazeh metagabbros. The possible mechanism of enrichment processes beneath the western part of the CEIM is discussed in the 6.6 section.

Petrogenesis of the Bayazeh metapicrite

According to the petrography and mineral chemistry, the Bayazeh metapicrites contains primary igneous clinopyroxenes (Figure 6F). Single clinopyroxene thermobarometry of Soesoo (1997) suggest temperatures of 1170 to 1220 ℃ and pressures ranging from 4.8 to 7.0 kbar (Nosouhian et al., 2014). The amounts of Al_2O_3 and TiO_2 in the clinopyroxenes indicate the magmatic pressures and temperature conditions (e.g. Wass, 1979).

Accordingly, the thermobarometry results and the wide range and positive correlation of TiO_2 and Al_2O_3 in the Bayazeh metapicrite clinopyroxenes (Table 3) indicate that clinopyroxene crystallization has been occurred during magma ascent (Nosouhian et al., 2014).

The chondrite-normalized REE patterns of the clinopyroxenes show that the LREEs are enriched relative to the HREEs (Figure 6G) and the $(Ce/Yb)_{CN}$ ratios are between 3.34 to 3.72. The LREEs have a convex upward pattern in the chondrite-normalized REE diagram (Figure 6G). This pattern suggests the nearly simultaneous crystallization of clinopyroxene and plagioclase from the magma that the LREEs prefer to inter in plagioclase structure more than in pyroxene one, during crystallization of these minerals (e.g. Ashchepkov and André, 2002, Nosouhian et al., 2014). The primitive mantle-normalized multi-element diagrams of clinopyroxenes indicate Ba, Th and U depletion, and Pb, Sr, Ti and Zr negative anomalies (Figure 6H). Negative Zr and Ti anomalies and low concentration of Rb, Ba, Th, U, Pb and Sr compared to primitive mantle of this mineral indicate that the melt crystallizing of clinopyroxene have a mantle origin (e.g. Wang and Gasparik, 2001; Nosouhian et al., 2014).

Picritic melts are produced by direct crystallization of high-Mg melts or less Mg-rich melts by accumulation of olivine (e.g. Tsikouras et al., 2008; Herzberg and O'Hara, 1998). The MgO content of the Bayazeh metapicrites does not represent the MgO content of a melt because a high amount of olivine (37-39 vol%) presents as accumulated crystals. These rocks in the MgO versus Cr diagram (Figure 8C) lie in the crystallization and accumulation of olivine field indicating the predominant role of olivine accumulation in the studied metapicrites. Also, the high amounts of Ni and Cr can be related to the olivine accumulation of these rocks. The high contents of Mg# and Ni reflect an olivine-bearing peridotite source rather than a pyroxenitic source for generation of this magma.

The high value of Cr with 1300 to 1431 ppm is recognized in the geochemical analyses of the Bayazeh metapicrite, but chromite mineral is absent in petrography. Based on the experimental result of Murck and Campble (1986), during the cooling of ultrabasic melts such as komatiite and picrite, olivine initially crystallizes alone and is joined by chromite only when the MgO content of the liquid falls to 25.0 wt% MgO (Nosouhian et al., 2014). The Bayazeh metapicrites have MgO contents of 25.8-28.0 wt% indicating that the chromium contents of these rocks are controlled by olivine crystallization (Figure 8C). Although the chemistry of Bayazeh metapicrite is controlled by cumulus olivine, the REE content in olivine are very low. Accordingly, they have not significantly affected to the REE composition of bulk rock.

All analyzed metapicrites in the chondrite and primitive mantle-normalized diagrams show parallel patterns implying that they were derived from a similar mantle source (Figure 7 C,D). The incompatible element abundances in these rocks reflect the composition of the parent magma (e.g. Zhang et al., 2017). Some studies have proposed models in which melts of picrite are generated at pressures higher than 2.5 GPa, implying a source within the garnet stability field (e.g., Woodland et al., 2002; Schuth et al., 2004; Nosouhian et al., 2014; Nironen 2017). The studied rocks are characterized by low Sm/Yb ratios (2.00-2.25) and low Yb contents (0.60-0.80 ppm) suggesting that garnet was absent in the melting source (Table 10). Also, the LREE enrichment relative to HREE, the $(La/Yb)_{CN}$ between 11.65 to 12.31, and the flat HREE pattern in the chondrite-normalized REE patterns does not favor garnet as a residual phase (Figure 7C). The flat HREE pattern explain melting started within the garnet stability field but continued in the spinel stability field as a result of continuing ascent of the mantle source (Tsikouras et al., 2008; Nosouhian et al., 2014; Nironen 2017). Therefore, the most suitable source for this magma is a mantle spinel peridotite.

The high HFSE abundances such as Nb, Ta, Zr and Hf in the primitive mantle-normalized diagram of the studied rocks requires the asthenospheric mantle source also to be rich in HFSE (Figure 7D). Primitive mantle-normalized diagram display the positive Ta and Nb, and negative Th, U and K anomalies (Figure 7D). Such patterns are typically observed in HIMU-like alkaline magmas (e.g. Willbold and Stracke, 2006). The negative K and positive Nb anomalies in this diagram (Figure 7D) and the unique MREE trends in the chondrite-normalized diagram (Figure 7C) show that the mantle source may have contained significant proportions of amphibole (e.g. Rollinson, 1993; Zhang et al., 1999). The presence of amphibole within the mantle is strong evidence that the asthenospheric mantle underwent metasomatic enrichment prior to melting. The metasomatic enrichment of the shallow mantle is principally ascribed to the release of fluids/melts from subduction zones (subduction models; e.g. Stein et al., 1997; Shaw et al., 2007) or by a rising plume (plume models; e.g. Beccaluva et al., 2009; Endress et al., 2011). Therefore, the studied rocks are generated by partial melting of a metasomatized asthenospheric amphibole-bearing spinel lherzolite.

The partial melting hypothesis was further tested by modeling of the REE during incongruent melting of a spinel-peridotite source (Rollinson, 1993). This model indicates that the Bayazeh metapicrites were generated by more than 40% partial melting of a mantle spinel peridotite (Nosouhian et al., 2014; Figure 8D). However, the mineralogical assemblage is effectively suggesting a H-bearing component, which may indicate the involvement

of fluids in the partial melting event. Hydrous melting can occur anytime a water-nearing component is melted in the asthenosphere. High water contents, in mantle regions, with lower solidus temperatures and induced partial melting at lower temperatures play an important role in the generation of picrite melts (e.g. Asahara et al., 1998). Also, phlogopite-bearing systems require the high water activity to remain stable (Esperanca and Holloway, 1987). Presence of primary phlogopite in the Bayazeh metapicrite is an evidence of a hydrated mantle source for generation of these rocks (Nosouhian et al., 2014). Geochemical characteristic of the studied metapicrites such as large variation of the LILE/HFSE ratio (e.g. Sr/Sm=61.33-107.86) and negative Ti anomaly associated with presence of phlogopite reveal the role of previously subducted oceanic crust. Accordingly, involvement of hydrous fluids related to subduction, enabled the peridotite source to melt despite the absence of abnormal thermal conditions. Therefore, the parental magma of the Bayazeh metapicrites has been derived from a high degree partial melting of a metasomatized spinel- and amphibole-bearing peridotite of the asthenospheric mantle (Nosouhian et al., 2014). The characteristic of the subducted oceanic crust in this part of the CEIM is discussed in the 6.6 section.

Petrogenesis of the amphibole-bearing listwaenite

Listwaenites are the silica-carbonate-rich products of low grade metasomatic processes affecting mafic and ultramafic rocks (e.g. Uçurum, 2000; Tsikouras et al., 2006). Listwaenitization process occurs after serpentinization of ultrabasic rocks (Nasir et al., 2007). Listwaenites are typically composed of quartz and carbonate minerals (magnesite, ankerite and dolomite), together with other accessory minerals such as chlorite, fuchsite, talc, chromite, magnetite and sulfides (Uçurum, 2000). They are commonly found in ophiolitic suites, along shear and/or fault zones that allow circulation of hydrothermal fluids, which cause metasomatism (e.g. Uçurum, 2000).

The Bayazeh amphibole-bearing listwaenites are mainly exposed along the shear and/or fault zones in the serpentinites and the transitional change of serpentinite to metamorphosed listwaenite is evident (Figure 4C). The lineation and foliation of these rocks are observed in the field study. The generation of metamorphosed listwaenites by effect of regional metamorphism on the ophicarbonites is rarely discussed (e.g., Taguchi et al., 2012; Nosouhian, 2016; Nosouhian et al., 2016b).

The mineral association of the studied listwaenites is represented by metamorphic amphiboles (tremolite and actinolite), carbonates (dolomite and calcite), quartz, serpentine (antigorite), chromian spinel, ferritchromite and chlorite (Figure 5 G,H). The chemical composition of

chromian spinel core in the Bayazeh amphibole-bearing listwaenites shows the high amount of Cr and Al, and low values of Fe^{3+} and Ti compared to the rims (Table 7). The rims are depleted in Al and Mg while, are enriched in Fe^{3+}, supporting their metamorphic origin (Table 7). The chromian spinel rims compared to the cores have the highest FeO[total] (50.79-53.12 wt%) and MnO (1.31-1.53 wt%) (Table 7), suggesting that Fe and to a lesser extend Mn are introduced into the chromian spinel during alteration and metamorphism (Taguchi et al., 2012; Pirnia et al., 2013; Nosouhian et al., 2016b). In the Cr-Al-Fe^{3+} ternary diagram, the chromian spinel cores of the studied metalistwaenites lie along the Cr-Al join and the outer rims plotted along the Cr-Fe^{3+} join in the ferritchromite (metamorphic) field (Nosouhian et al., 2016b; Figure 6D).

The unique petrological characteristic of the Bayazeh ophiolite is due to regional metamorphism, which produced metalistwaenites by carbonation of serpentinites (Nosouhian et al., 2016b). Several pieces of evidence indicate that the studied listwaenites likely formed during regional metamorphism of an ultramafic protolith (Nosouhian et al., 2016b). These include: (1) the studied rocks display lineation and foliation along the shear and/or fault zones. (2) these rocks are composed of metamorphic amphiboles (tremolite and actinolite), carbonates (dolomite and calcite), quartz and serpentine together with chromian spinel, ferritchromite and chlorite; the presence of chromian spinel and serpentine in the metalistwaenites indicates an ultramafic protolith; (3) high amounts of amphiboles (tremolite and actinolite) with metamorphic nature which are present in these rocks; (4) XRD patterns of the studied rocks suggest that the serpentine polytype is antigorite; (5) ferritchromite is present in the outer rim of some chromian spinels. Ferritchromite is produced as a consequence of metamorphism (e.g. Barnes, 2000; Merlini et al., 2009); (6) the chlorite in the rim of some chromian spinels is produced at relatively high temperature (Kimball, 1990).

The phase relationships of this siliceous carbonated ultramafic rock may be discussed in the P-T-XCO_2 space for the CaO-MgO-SiO_2-CO_2-H_2O system (Trommsdorff and Evans, 1974, 1977). The T-XCO_2 diagram is shown in Figure 8E that the dashed line represents a metamorphic assemblage in the studied listwaenites; Antigorite+Calcite=Tremolite+Dolomite. This diagram reveals temperatures of approximately 488 to 497 °C at a 3.5 kbar fluid pressure for the amphibole-bearing listwaenite, which indicates upper greenschist to lower amphibolite facies P-T conditions (Nosouhian et al., 2016b).

The petrological characteristic of these rocks, and presence of tremolite, actinolite, antigorite, dolomite, calcite, quartz, chromian spinel and ferritchromite,

together with the field relationships with their host serpentinites, suggest that the studied metalistwaenites formed by a textural and compositional modification during alteration processes and regional metamorphism from the carbonation of serpentinites (Nosouhian et al., 2016b).

Sub-solidus evolutions in the Bayazeh ophiolite

In the Bayazeh serpentinite and metapicrite, olivine was the main mineral, although now completely altered to serpentine. Serpentine mineral is identified as antigorite, based on the X-ray diffraction analysis. Antigorite is present in the serpentinite, amphibole-bearing listwaenite and metapicrite. This mineral occurs mostly as fine-grained crystals that partly changed to the metamorphosed tremolite (e.g. Scotford and Williams, 1983). The typical succession of serpentine minerals with increasing metamorphic grade is lizardite-chrysotile-antigorite (Moody, 1976). Accordingly, antigorite is thought to be a prograde product of the lizardite and chrysotile during regional metamorphism (Moody, 1976), that the upper stability limit of antigorite lies between 500 °C and 600 °C (Spear, 1995).

Primary chromian spinels are partly altered to ferritchromite and magnetite at their margins in the serpentinites and metalistwaenites. Metamorphic modifications of chromian spinel have been frequently described in the several literatures (e.g. Barnes, 2000; Taguchi et al., 2012; Pirnia et al., 2013). Based on the mineral chemistry of chromian spinels, the degree of exchange and replacement reactions in this mineral is generally related to the metamorphic fluid access and fluid-rock ratios. If the fluid-rock interaction is intense, the chromian spinel will be almost completely destroyed (Barnes, 2000). The preservation of unaltered chromian spinel cores in the serpentinite indicates a small degree of fluid-rock interaction. On the other hand, chromian spinel cores in the metalistwaenites contain higher FeO^{total}, TiO_2 and MnO, and lower Cr_2O_3 and Al_2O_3 compared to the chromian spinel cores in the serpentinites (Table 7). These chemical characteristics and the presence of chlorite around the spinels in the metalistwaenites indicate a high fluid-rock ratio interaction and low-grade metamorphism.

Some chromian spinel rims in the metalistwaenites are replaced by chlorite (Figure 5 G,H). This chlorite presents high contents of Cr_2O_3 (2.78-3.17 wt%), MgO (21.66-23.14 wt%) and Al_2O_3 (16.34-16.89 wt%) (Table 8), implying that chromian spinel could have supplied the Cr_2O_3, MgO and Al_2O_3 necessary for the formation of chlorite (Hamdy and Lebda, 2011). Kimball (1990) proposed that the Mg- and Al- rich components of the primary chromian spinel would have reacted with MgO and SiO_2 rich fluids to produce chlorite around the chromian spinels at a relatively

high temperature (>400 °C).

The thermodynamic stability of the spinel solid solution as a function of temperature, oxygen fugacity and the composition of coexisting olivine is discussed by Sack and Ghiorso (1991). In this thermodynamic model, the ferritchromite compositions in the studied metalistwaenite lie along the Cr-Fe^{3+} join, corresponding to metamorphism under upper greenschist to lower amphibolite facies P-T conditions at around 550 °C (Figure 8F). This chemical variation is typical of chromian spinel altered in greenschist facies (Evans and Frost, 1975; Suita and Strieder, 1996) or lower amphibolite facies P-T conditions (Arai et al., 2006). Furthermore, the serpentine minerals associated with ferritchromites appear to be antigorite, formed during prograde regional metamorphism. Jan and Windley (1990) assumed that the formation of ferritchromite, antigorite and high-mg chlorite is occurred in the minimum temperature at around 500 °C. Also, in the CaO-MgO-SiO_2-CO_2-H_2O system, the phase relationships of the metamorphosed listwaenites reveal temperatures of approximately 488 to 497 °C at a 3.5 kbar fluid pressure that this condition indicates the upper greenschist to lower amphibolite facies P-T conditions. As mentioned above, the mineral assemblage of the Bayazeh rock units and the composition of the chromian spinels in the amphibole-bearing listwaenites concur with the effects of regional metamorphism in the upper greenschist to lower amphibolite facies P-T conditions.

Based on the new geochronological ages and reconstruction, Bagheri (2007), and Bagheri and Stampfli (2008) conclude that the region south of the Great Kavir Fault between the Great Kavir and the Bayazeh Faults underwent metamorphism during the Carboniferous (Variscan event) and also subsequent deformation during Permian and Triassic. The first phase was limited to greenschist-amphibolite facies conditions and the second phase was a retrograde in greenschist facies. Accordingly, the Variscan event may have been responsible for the Paleozoic age metamorphism of the Yazd block (study area), which was followed by retrograde metamorphism under greenschist facies condition.

Geotectonic Setting

The occurrence of the Anarak, Jandaq, Bayazeh and Posht-e-Badam Paleozoic ophiolites in the western part of the Central-East Iranian Microcontinent propounds many questions about the evolution and the number of Paleo-Tethys sutures between Eurasian and Iran (Zanchi et al., 2009). Previous studies suggested a post-Triassic 135° anti-clockwise rotation of the Central Iran transferring a large fragment of the Paleo-Tethys suture from the present-day Afghanistan-Iran border to Central Iran (e.g. Davoudzadeh, 1997). But, palaeomagnetic data of the

Nakhlak Triassic succession by Muttoni et al. (2009), Late Triassic palaeomagnetic data of Besse et al. (1998), fauna studies by Balini et al. (2009), and regional facies analysis of Upper Silurian-Lower Carboniferous successions by Wendt et al. (2005), do not support this idea. Torabi (2011), on the base of new geological data, concluded that the presence of Paleozoic ophiolites along the main faults of central and northern Iran points to multi-suture closure of the Paleo-Tethys Ocean in Late Paleozoic to Early Mesozoic times.

The geological history and position of the Bayazeh area (study area) within the Central-East Iranian Microcontinent can be related to the Paleo-Tethys Ocean. Based on the evolution of the CEIM including the study area, the Anarak, Jandaq, Bayazeh and Posht-e-Badam ophiolites are likely related to the initial opening and subduction of the Paleo-Tethys Ocean (Bagheri and Stampfli, 2008; Torabi et al., 2011; Nosouhian, 2016). Paleo-Tethys Ocean started with a Late Ordovician-Early Devonian rifting and terminated in the Triassic with the Eocimmerian collision (Bagheri and Stampfli, 2008). Subduction of Paleo-Tethys is a possible cause of the volatile enrichment of the mantle in Upper Paleozoic. Therefore, Paleo-Tethys subduction from the Early to the Late Paleozoic was the probable cause of volatile enrichment and mantle metasomatism (Torabi and Hemmati, 2011; Torabi, 2012).

The melt generation in the mantle wedge is produced by dehydration reactions within subduction oceanic crust and sediments (e.g. Ringwood, 1974), and the LILE-enriched fluid phases released from the subducted slab and/or sediments into the mantle wedge are discussed in the literatures (e.g. Hawkesworth et al., 1991; Tonerini et al., 2001). For instance, this study shows that the Bayazeh metapicrites and metagabbros indicate selective enrichment of the mobile elements such as Cs, Rb and Ba compared to HFSE and REE (Figure 7 B,D). The marked enrichments in Cs relative to Rb suggest that metasomatic agents were fluid phases, most plausibly derived from a subducting slab (e.g. Tonarini et al., 2001). Positive anomalies and high values of the fluid mobile elements (e.g. Cs, Rb, Ba) in the studied rocks from the Bayazeh ophiolite define the aqueous fluid released at low temperatures (i.e., usually shallow) from subducted crust or sediment (e.g. Pearce and Stern, 2006).

CONCLUSION

The western part of the Central-East Iranian Microcontinent (CEIM) hosts the Anarak, Jandaq, Bayazeh and Posht-e-Badam ophiolites of Paleozoic age. The Bayazeh ophiolite is found as a sheared and metamorphosed tectonic mélange in the Eastern margin of the Yazd block. This ophiolite consists of serpentinized peridotites, metagabbro, metapicrite, serpentinite and metalistwaenite, which are covered by Late Paleozoic schist and marble. All the litological units underwent a prograde metamorphism under upper greenschist to lower amphibolite facies P-T conditions, which was followed by retrograde metamorphism under greenschist facies conditions.

Mineral chemistry of preserved chromian spinel cores in the Bayazeh serpentinites indicates high values of Cr# (60.67-67.59) and Mg, and low contents of Fe^{3+} and Ti, this confirming their mantle nature. The chemical characteristics of the investigated chromian spinels suggest an ophiolitic origin and a high degree of partial melting of mantle harzburgites in a supra-subduction zone geotectonic setting.

The Bayazeh amphibole-bearing listwaenites are commonly found along the shear and/or fault zones within the serpentinites in the field observations. The unique petrological characteristic of this ophiolite is due to regional metamorphism, which produced metalistwaenites by carbonation of serpentinites. The texture and mineral assemblage of the amphibole-bearing listwaenites and the chemical composition of the chromian spinel reveal that these rocks underwent a prograde metamorphism under upper greenschist to lower amphibolite facies P-T conditions.

The geochemical characteristics of the Bayazeh metagabbros indicate enrichment of LILE and U compared to HFSE suggesting the protolith is a cumulate gabbro rather than a noncumulate (isotropic) gabbro. The enrichment of LILE compared to HFSE and depletion of Nb and Ti relative to other HFSE indicate involvement of subduction component in the depleted mantle source, and suggest that these rocks are generated in a subduction setting. Therefore, the Bayazeh metagabbros are produced by high degree partial melting of lithospheric mantle that was previously enriched in incompatible elements related to the subducted slab.

The Bayazeh metapicrites are characterized by high MgO, Ni and Cr contents indicating the predominant role of olivine (37-39 vol%) accumulation in these rocks. Although the chemistry of Bayazeh metapicrite is controlled by cumulus olivine, the REE content in olivine are very low and the whole rock compositions of these rocks can be used to the mantle-derived melt. Enrichment of HFSE and LREE (e.g. $[La/Yb]_{CN}$=11.65-12.31), associated with a large variation of LILE concentrations indicate metasomatic enrichment of an asthenospheric mantle source with a subduction-related components prior to melting. The presence of phlogopite as a primary hydrous mineral together with high LILE/HFSE ratios and a negative Ti anomaly reveal the role of previously subducted oceanic crust. Geochemical characteristics of the studied metapicrites show that they were generated

by high degree partial melting of a metasomatized asthenospheric amphibole-bearing spinel lherzolite. Subduction of the Paleo-Tethys from the Early to the Late Paleozoic is the cause of volatile enrichment and mantle metasomatism.

REFERENCES

Abdel-Fattah M., Abdel-Rahman A.M., Nassar P.E., 2004. Cenozoic volcanism in the Middle East: petrogenesis of alkali basalts from Northern Lebanon. Geological Magazine 141, 545-563.

Aistov L., Melnikov B., Krivyakin B., Morozov L., 1984. Geology of the Khur Area (Central Iran). Report NO. 20, Geological Survey of Iran, Iran, 132 pp.

Alici Sen P., Temel A., Gourgaud A., 2004. Petrogenetic modeling of Quaternary post-collisional volcanism: a case study of central and eastern Anatolia. Geological Magazine 141, 81-98.

Arai S., 1994. Characterization of spinel peridotite by olivine-spinel compositional relationships: review and interpretation. Chemical Geology 113, 191-204.

Arai S., Okamura H., Kadoshima K., Tanaka C., Suzuki K., Ishimaru S., 2011. Chemical characteristics of chromian spinel in plutonic rocks: implications for deep magma processes and discrimination of tectonic setting. Island Arc 20, 125-137.

Arai S., Shimizu Y., Ismail S.A., Ahmed A.H., 2006. Low-T formation of high-Cr spinel with apparently primary chemical characteristics within podiform chromitite from Rayat, northeastern Iraq. Mineralogical Magazine 70, 499-508.

Arndt N.T., 2008. Komatiite. Cambridge University Press, Cambridge, London, 467 pp.

Arvin M. and Robinson P.T., 1994. The petrogenesis and tectonic setting of lavas from the Baft ophiolitic melange, southwest of Kerman, Iran. Canadian Journal of Earth Sciences 31, 824-834.

Asahara Y., Ohtani E., Suzuki A., 1998. Melting relations of hydrous and dry mantle compositions and the genesis of komatiites. Geophysical Research Letters 25, 2201-2204.

Ashchepkov I.V. and André L., 2002. Pyroxenite xenoliths in picrite basalts (Vitim Plateau): origin and differentiation of mantle melts. Russian Geology and Geophysics 43, 343-363.

Bagheri S., 2007. The exotic Paleo-Tethys terrane in Central Iran: new geological data from Anarak, Jandaq and Posht-e-Badam areas. Ph.D. Thesis, Faculty of Geosciences and Environment, University of Lausanne, Switzerland, 208 pp.

Bagheri S. and Stampfli G.M., 2008. The Anarak, Jandaq and Posht-e-Badam metamorphic complexes in central Iran: new geological data, relationships and tectonic implication. Tectonophysics 451, 123-155.

Balini M., Nicora A., Berra F., Garzanti E., Levera M., Mattei M., Muttoni G., Zanchi A., Bollati I., Larghi C., Zanchetta S., Salamati R., Mossavvari F., 2009. The Triassic stratigraphic succession of Nakhlak (Central Iran), a record from an active margin. In: South Caspian to Central Iran basins. (Eds.): M.F. Brunet, M. Wilmsen, J.W. Granath, Geological Society of London, Special Publication, London, UK 312, 287-321.

Barnes S.J., 2000. Chromite in Komatiites: II. Modifications during greenschist to mid amphibolite facies metamorphism. Journal of Petrology 41, 387-409.

Barnes S.J. and Roeder P.L., 2001. The range of spinel compositions in terrestrial mafic and ultramafic rocks. Journal of Petrology 42, 2279-2302.

Bayat F. and Torabi G., 2011. Alkaline lamprophyric province of Central Iran. Island Arc 20, 386-400.

Beccaluva L., Bianchini G., Natali C., Siena F., 2009. Continental flood basalts and mantle plumes: a case study of the Northern Ethiopian Plateau. Journal of Petrology 50, 1377-1403.

Berger J., Femenias O., Mercier J.C.C., Demaiffe D., 2005. Ocean-floor hydrothermal metamorphism in the Limousin ophiolites (western French Massif Central): evidence of a rare preserved Variscan oceanic marker. Journal of metamorphic Geology 23, 795-812.

Besse J., Torcq F., Gallet Y., Ricou L.E., Krystyan L., Saidi A., 1998. Late Permian to late Triassic paleomagnetic data from Iran: constraints on migration of the Iranian block through the Tethyan Ocean and initial destruction of Pangea. Geophysical Journal International 135, 77-92.

Davoudzadeh M., 1997. Geology of Iran. In: Encyclopedia of Asian and European Regional Geology. (eds): E.M. Moores and R.W. Fairbridge, Chapman & Hall, UK, 384-405.

Deer W.A., Howie R.A., Zussman J., 1992. An introduction to the rock forming minerals. Longman, London, UK, 528 pp.

Dick H.J.B. and Bullen T., 1984. Chromian spinel as a petrogenetic indicator in abyssal and alpine-type peridotites and spatially associated lavas. Contributions to Mineralogy and Petrology 86, 54-76.

Droop G.T.R., 1987. A general equation for estimating Fe^{3+} concentrations in ferromagnesian silicates and oxides from microprobe analyses, using stoichiometric criteria. Mineralogical Magazine 51, 431-435.

Endress C., Furman T., Abu El-Rus M.A.A., Hanan B.B., 2011. Geochemistry of 24 Ma basalt from NE Egypt: source components and fractionation history. Geological Society of London Special Publication 357, 265-283.

Esperanca S. and Holloway J.R., 1987. On the origin of some mica lamprophyres: experimental evidence from a mafic minetta. Contributions to Mineralogy and Petrology 95, 207-216.

Evans B.W. and Frost B.R., 1975. Chrome-spinel in progressive metamorphism: a preliminary analysis. Geochimica et

Cosmochimica Acta 39, 959-972.

Farahat E.S., 2008. Chrome-spinels in serpentinites and talc carbonates of the El Ideid-El Sodmein District, central Eastern Desert, Egypt: their metamorphism and petrogenetic implications. Chemie der Erde, Geochemistry 68, 193-205.

Gansser A., Gupta H.K., Delany F.M., 1981. The geodynamic history of the Himalaya, Zagros, Hindu Kush, Himalaya; geodynamic evolution. Geodynamics 3, 111-121.

Hamdy M.M. and Lebda E.M., 2011. Al-compositional variation in ophiolitic chromitites from the south Eastern Desert of Egypt: petrogenetic implications. Journal of Geology and Mining Research 3, 232-250.

Herzberg C. and O'Hara M.J., 1998. Phase equilibrium constraints on the origin of basalts, picrites, and komatiites. Earth Science Reviews 44, 39-79.

Hassanipak A.A. and Ghazi A.M., 2000. Petrology, geochemistry and tectonic setting of the Khoy ophiolite, northwest Iran: implications for Tethyan tectonics. Journal of Asian Earth Sciences 18, 109-121.

Hawkesworth C.J., Hergt J.M., McDermott F., Ellam R.M., 1991. Destructive margin magmatism and the contributions from the mantle wedge and subducted crust. Australian Journal of Earth Sciences 38, 577-594.

Hellebrand E., Snow E.J., Dick H.J.B., Hofmann A.W., 2001. Coupled major and trace elements as indicators of the extent of melting in mid-ocean-ridge peridotites. Nature 410, 677-681.

Hey M.H., 1954. A new review of the chlorites. Mineralogical Magazine 30, 277-292.

Jan M.Q. and Windley B.F., 1990. Chromian spinel-silicate chemistry in ultramfic rocks of the Jijal Complex, northwest Pakistan. Journal of Petrology 31, 67-71.

Kamenetsky V., Crawford A.J., Meffre S., 2001. Factors controlling chemistry of magmatic spinel: an empirical study of associated olivine, Cr-spinel and melt inclusions from primitive rocks. Journal of Petrology 42, 655-671.

Kimball K.L., 1990. Effects of hydrothermal alteration on the composition of chromian spinels. Contributions to Mineralogy and Petrology 105, 337-346.

Le Bas M.J., 2000. IUGS reclassification of the high-Mg and picritic volcanic rocks. Journal of Petrology 41, 1467-1470.

McDonough W.F., 1990. Constraints on the composition of the continental lithospheric mantle. Earth and Planetary Science Letters 101, 1-18.

McDonough W.F. and Frey F.A., 1989. REE in upper mantle rocks. In: Geochemistry and mineralogy of rare earth elements. (eds): B. Lapin and G.R. McKay, Mineralogical Society of America, Michigan, 99-145 pp.

McDonough W.F. and Sun S.S., 1995. The composition of the earth. Chemical Geology 120, 223-253.

McLennan S.M. and Taylor S.R., 1991. Sedimentary rocks and crustal evolution: tectonic setting and secular trends. Journal of Geology 99, 1-21.

Merlini A., Grieco G., Diella V., 2009. Ferritchromite and chromian-chlorite formation in mélange-hosted Kalkan chromitite (Southern Urals, Russia). American Mineralogist 94, 1459-1467.

Miyashiro A., 1973. The Troodos ophiolitic complex was probably formed in an island arc. Earth and Planetary Science Letters 19, 218-224.

Moody J.B., 1976. Serpentinization: a review. Lithos 9, 125-138.

Morimoto N., 1989. Nomenclature of pyroxenes. The Canadian Mineralogist 27, 143-156.

Morishita T., Ishida Y., Arai S., 2005. Simultaneous determination of multiple trace element compositions in thin (<30 μm) layers of BCR-2G by 193 nm ArF excimer laser ablation-ICP-MS: implications for effect and elemental fractionation on quantitative analysis. Geochemical Journal 39, 327-340.

Murck B.W. and Campble I.H., 1986. The effects of temperature, oxygen fugacity and melt composition of the behaviour of chromium in basic and ultrabasic melts. Geochimica et Cosmochimica Acta 50, 1871-1887.

Muttoni G., Mattei M., Balini M., Zanchi A., Gaetani M., Berra F., 2009. The drift history of Iran from the Ordovician to the Triassic. Geological Society of London 312, 7-29.

Nasir S., Al Sayigh A.R., Al Harthy A., Al Khirbash S., Al Jaaidi O., Musllam A., Al Mishwat A., Al Busaidi S., 2007. Mineralogical and geochemical characterization of listwaenite from the Semail ophiolite, Oman. Chemie der Erde, Geochemistry 67, 213-228.

Nironen M., 2017. The Salittu Formation in southwestern Finland, part II: Picritic-basaltic volcanism in mature arc environment. Bulletin of the Geological Society of Finland 89, 5-19.

Nosouhian N., 2016. Petrology of the Paleozoic metaophiolite and Mesozoic felsic dykes swarm in the west and southwest of the Bayazeh (South of Khur- Central Iran). Ph.D. Thesis, University of Isfahan, Isfahan, Iran, 270 pp.

Nosouhian N., Torabi G., Arai S., 2014. Metapicrites of the Bayazeh ophiolite (Central Iran), a trace of Paleo-Tethys subduction-related mantle metasomatism. Neues Jahrbuch für Geologie und Paläontologie, Abhandlungen 271, 1-19.

Nosouhian N., Torabi G., Arai S., 2016a. Late Cretaceous dacitic dyke swarm from Central Iran, a trace for amphibolite melting in a subduction zone. Geotectonics 50, 295-312.

Nosouhian N., Torabi G., Arai S., 2016b. Amphibole-bearing listwaenites from the Paleozoic Bayazeh ophiolite (Central Iran). Italian Journal of Geosciences 135, 109-119.

Pal T. and Mitra S., 2004. P-T-fO$_2$ controls on a partly inverse chromite-bearing ultramafic intrusive: an evaluation from the Sukinda Massif, India. Journal of Asian Earth Science 22, 483-493.

Pearce J.A., Lippard S.J., Roberts S., 1984. Characteristics and tectonic significance of suprasubduction zone ophiolites. In: Marginal basin geology. (eds): B.P. Kokiaar and M.F.

Howells, Geological Society of London, Special Publication, UK, 77-94.

Pearce J.A. and Stern R.J., 2006. Origin of back-arc basin magmas: trace element and isotopic perspectives. In: Back-arc spreading system: geological, biological, chemical, and physical interactions. (Eds.): D.M. Christie, C.R. Fisher, S.M. Lee, S. Givens, Geophysical Monograph Series, American Geophysical Union, 63-86.

Pirnia T, Arai S., Torabi G., 2013. A better picture of the mantle section of the Nain ophiolite inferred from detrital chromian spinels. Journal of Geology 121, 645-661.

Pomonis P. and Magganas A., 2017. Petrogenetic implications for ophiolite ultramafic bodies from Lokris and Beotia (Central Greece) based on chemistry of their Cr-spinels. Geosciences 7, 1-16.

Qiu R.Z., Zhou S., Li T.D., Deng J.F., Xiao Q.H., Wu Z.X., Cai Z.Y., 2006. The tectonic setting of ophiolites in the western Qinghai-Tibet Plateau, China. Journal of Asian Earth Science 29, 215-228.

Reichert J., 2007. A metallogenetic model for carbonate-hosted non-sulphide zinc deposits based on observations of Mehdi Abad and Irankuh, central and southwestern Iran. Ph.D. Thesis, Martin-Luther University, Halle-Wittenberg, Germany, 157 pp.

Ringwood A.E., 1974. The petrological evolution of island arc systems. Journal of the Geological Society of London 130, 183-204.

Rollinson H.R., 1993. Using geochemical data: evaluation, presentation, interpretation. UK: Longman Scientific and Technical Publishers, London, 352 pp.

Sack R.O. and Ghiorso M.S., 1991. Chromian spinels as petrogenetic indicators: thermodynamic and petrological applications. American Mineralogist 76, 827-847.

Schuth S., Rohrbach A., Münker C., Ballhaus C., Garbe-Schnberg D., Qopoto C., 2004. Geochemical constraints on the petrogenesis of arc picrites and basalts, New Georgia Group, Solomon Islands. Contributions to Mineralogy and Petrology 148, 288-304.

Scotford D.M. and Williams J.R., 1983. Petrology and geochemistry of metamorphosed ultramafic bodies in a portion of the Blue ridge of North Carolina and Virginia. American Mineralogist 68, 78-94.

Shaw J.E., Baker J.A., Kent J.R.; Ibrahim K.M., Menzies M.A., 2007. The Geochemistry of the Arabian Lithospheric Mantle-a Source for intraplate volcanism? Journal of Petrology 48, 1495-1512.

Shervais J.W., 2001. Birth, death, and resurrection: the life cycle of suprasubduction zone ophiolites. Geochemistry, Geophysics, Geosystems 2, 2000GC000080.

Shkoľnik S.I., Reznitsky L.Z., Barash I.G., 2011. Possibility of identification of back-arc paleobasins from high-grade orthometamorphite rocks: evidence from basic crystalline schists of the Slyudyanka crystalline complex, South Baikal

region. Geochemistry International 49, 1177-1194.

Soesoo A., 1997. A multivariate statistical analysis of clinopyroxene composition: empirical coordinates for the crystallisation PT-estimations. Geologiska Föreningen i Stockholm Förhandlingar 119, 55-60.

Spear F.S., 1995. Metamorphic phase equilibria and pressure-temperature-time paths. Mineralogical Society of America, Washington. 799 pp.

Stalder R., Foley S., Brey G.P., Horn I., 1998. Mineral aqueous fluid partitioning of trace elements at 900-1200 °C and 3.0-5.7 GPa: new experimental data for garnet, clinopyroxene and rutile and implications for mantle metasomatism. Geochimica et Cosmochimica Acta 62, 1781-1801.

Stein M., Navon O., Kessel R., 1997. Chromatographic metasomatism of the Arabian Nubian lithosphere. Earth and Planetary Science Letters 152, 75-91.

Stockin J., 1968. Structural history and tectonics of Iran, a review. Bulletin of the American Association of Petroleum Geologists 52, 1229-1258.

Suita M.T.F. and Strieder A.J., 1996. Cr-spinels from Brazilian mafic-ultramafic complexes: metamorphic modifications. International Geology Review 38, 245-267.

Sun S.S. and McDonough W.F., 1989. Chemical and isotopic systematics of oceanic basalts: implications for mantle composition and processes. In: Magmatism in the ocean basin. (Eds.): A.D. Saunders and M.J. Norry, Geological Society of London, Special Publication, UK, 313-346.

Taguchi T., Satish-Kumar M., Hokada T., Jayananda M., 2012. Petrogenesis of Cr-rich calc-silicate rocks from the Bandihalli supracrustal belt, Archean Dharwar Craton, India. The Canadian Mineralogist 50, 705-718.

Tonarini S., Armienti P., D'Orazio M., Innocenti F., 2001. Subduction-like fluids in the genesis of Mt. Etna magmas: evidence from boron isotopes and fluid mobile elements. Earth and Planetary Science Letters 192, 471-483.

Torabi G., 2011. Late Permian blueschist from Anarak ophiolite (Central Iran, Isfahan province), a mark of multi-suture closure of the Paleo-Tethys Ocean. Revista Mexicana de Ciencias Geologicas 28, 544-554.

Torabi G., 2012. Late Permian post-ophiolitic trondhjemites from Central Iran: a mark of subduction role in growth of Paleozoic continental crust. Island Arc 21, 215-229.

Torabi G., 2013. Chromitite absence, presence and chemical variety in ophiolites of the Central Iran (Naein, Ashin, Anarak and Jandaq). Neues Jahrbuch für Geologie und Paläontologie, Abhandlungen 267, 171-192.

Torabi G. and Arai S., 2013. Back-arc Paleo-Tethys related blueschist from Central Iran (South of Chupanan, Isfahan Province). Petrology 18, 393-407.

Torabi G. and Hemmati O., 2011. Alkaline basalt from the Central Iran, a mark of previously subducted Paleo-Tethys Oceanic crust. Petrology 19, 690-704.

Torabi G., Arai S., Koepke J., 2011. Metamorphosed mantle

peridotites from Central Iran (Jandaq area, Isfahan province). Neues Jahrbuch für Geologie und Paläontologie, Abhandlungen 261, 129-150.

Trommsdorff V. and Evans B.W., 1974. Alpine metamorphism of peridotite rocks. Schweizerische Mineralogische und Petrographische Mitteilungen 56, 79-93.

Trommsdorff V. and Evans B.W., 1977. Antigorite-ophicarbonates: contact metamorphism in Valmalenco, Italy. Contributions to Mineralogy and Petrology 62, 301-312.

Tsikouras B., Karipi S., Grammatikopoulos T.A., Hatzipanagiotou K., 2006. Listwaenite evolution in the ophiolite mélange of Iti Mountain (continental Central Greece). European Journal of Mineralogy 18, 243-255.

Tsikouras B., Pe-Piper G., Piper D.J.W., Hatzipanagiotou K., 2008. Triassic rift-related komatiite, picrite and basalt, Pelagonian continental margin, Greece. Lithos 104, 199-215.

Uçurum A., 2000. Listwaenites in Turkey: perspectives on formation and precious metal concentration with reference to occurrences in East-Central Anatolia. Ofioliti 25, 15-29.

Van Hinsbergen D.J.J., Peters K., Maffione M., Spakman W., Guilmette C., Thieulot C., Plumper O., Gurer D., Brouwer F.M., Aldanmaz E., Kaymakcı N., 2015. Dynamics of intraoceanic subduction initiation: 2. Suprasubduction zone ophiolite formation and metamorphic sole exhumation in context of absolute plate motions. Geochemistry, Geophysics, Geosystems 16, 1771-1785.

Veblen D.R. and Ribbe P.H., 1982. Amphiboles: petrology and experimental phase relations. Mineralogical Society of America, Reviews in Mineralogy, 390 pp.

Wakabayashi J., Ghatak A., Basu A.R., 2010. Suprasubduction-zone ophiolite generation, emplacement, and initiation of subduction: a perspective from geochemistry, metamorphism, geochronology, and regional geology. Geological Society of America 122, 1548-1568.

Wang W. and Gasparik T., 2001. Metasomatic clinopyroxene inclusions in diamonds from the Liaoning province, China. Geochimica et Cosmochimica Acta 65, 611-620.

Wass S.Y., 1979. Multiple origins of clinopyroxenes in alkali basaltic rocks. Lithos 12, 115-132.

Wendt J., Kaufmann B., Belka Z., Farsan N., Karimi Bavandpour A.R., 2005. Devonian/Lower Carboniferous stratigraphy, facies patterns and palaeogeography of Iran, part II. Northern and Central Iran. Acta Geologica Polonica 55, 31-97.

Whitney D.L. and Evans B.W., 2010. Abbreviations for names of rock-forming minerals. American Mineralogist 95, 185-187.

Willbold M. and Stracke A., 2006. Trace element composition of mantle end-embers: implications for recycling of oceanic and upper and lower continental crust. Geochemistry Geophysics Geosystems 7, doi: 10.1029/2005GC001005.

Woodland S.J., Pearson D.G., Thirlwall M.F., 2002. A platinum group element and Re-Os isotope investigation of siderophile element recycling in subduction zones: comparison of

Grenada, Lesser Antilles Arc, and the Izu-Bonin Arc. Journal of Petrology 43, 171-198.

Zanchi A., Zanchetta S., Garzanti E., Balini M., Berra F., Mattei M., Muttoni G., 2009. The Cimmerian evolution of the Nakhlak-Anarak area, Central Iran, and its bearing for the reconstruction of the history of the Eurasian margin. Geological Society of London 312, 261-286.

Zhang M., OʹReilly S.Y., Chen D.G., 1999. Location of Pacific and Indian mid-ocean ridge-type mantle in two time slices, evidence from Pb, Sr and Nd isotopes for Cenozoic Australian basalts. Geology 27, 39-42.

Zhang Y., Song S., Yang L., Su L., Niu Y., Allen M.B., Xu X., 2017. Basalts and picrites from a plume-type ophiolite in the South Qilian Accretionary Belt, Qilian Orogen: Accretion of a Cambrian Oceanic Plateau? Lithos 278, 97-110.